Overturning circulation that ventilates the intermediate layer of the Sea of Okhotsk and the North Pacific
（オホーツク海と北太平洋の中層を通気するオーバーターン循環）

Junji Matsuda

松田 淳二
北海道大学大学院 環境科学院 地球圏科学専攻
大気海洋物理学・気候力学コース

May 12, 2014

Abstract

Dense Shelf Water (DSW) formation in the northwestern continental shelf in the Sea of Okhotsk is the beginning of the lower limb of the overturning circulation that ventilates the intermediate layer of the North Pacific Ocean. The upper limb consisting of surface currents in the Okhotsk Sea and the subarctic gyre has been identified only vaguely. Using a high resolution North Pacific Ocean model with a curvilinear grid as fine as 3km $\times$ 3km in the Sea of Okhotsk, we succeeded in representing the three-dimensional structure of the overturning circulation including the narrow boundary currents and flows through straits that constitute the upper limb, as well as the lower limb consisting of DSW formation and ventilation. In particular, pathways and timescales from the Bering Sea to the intermediate layer via the ventilation in the Sea of Okhotsk were examined in detail using tracer experiments. Further, we found that the overturning circulation that connects surface and intermediate layer is sensitive to wind stress. In case of strong winds, the coastal current under polynyas where DSW forms is intensified, and consequently diapycnal transport from the surface layer to the intermediate layer increases. Strong winds also induce positive sea surface salinity anomaly in the subarctic region, causing a significant decrease in the density stratification and increase in the DSW salinity (i.e. density). These processes act together to allow intense overturning circulation and deep ventilation, which may subduct even to the bottom of the Sea of Okhotsk if the wind is extremely strong. We also examined the sensitivity to fresh water flux and found that salinity variations in the eastern Bering Sea propagates to the Sea of Okhotsk, and affects SSS in the Sea of Okhotsk and then overturning circulation.

1 Introduction

Vigorous sea ice production occurs over the northwestern shelf in the Sea of Okhotsk (Fig. 1) due to the cold outbreak from the Eurasian Continent in winter. Cold and saline dense shelf water (DSW) forms there as a product of the sea ice formation [Kitani, 1973; Shcherbina, 2003]. DSW intrudes into the intermediate layer at the depth ranging between 200 m and 500 m in the Sea of Okhotsk and finally becomes a source of North Pacific Intermediate Water (NPIW) characterized by the local minimum of salinity [Talley, 1991; Yasuda et al., 1996]. This constitutes the lower limb of the intermediate overturning circulation [Talley, 2003] connecting the surface layer to the intermediate layer of the North Pacific (Fig. 2).

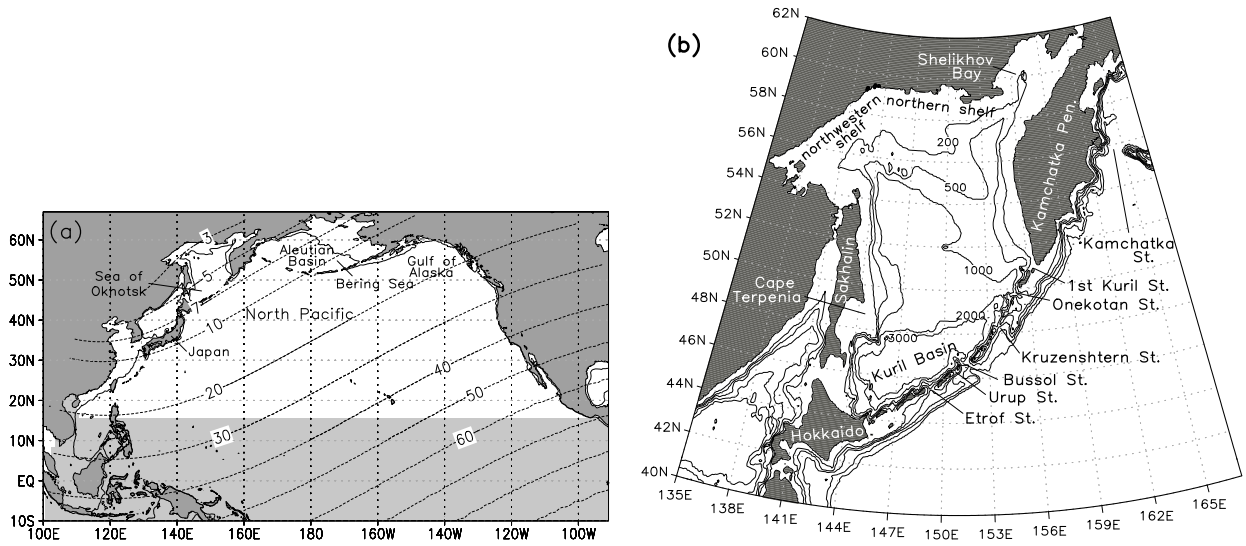

Figure 1: (a) Model domain. Model resolution (km, contour), restoring area (shaded), and bathymetric contour of 200 m are shown. Restoring areas are south of 15°N, east of 110°E, west of 90°W in the North Pacific, and north of 65°N in the Arctic Ocean. (b) Detailed model topography around the Sea of Okhotsk. Bathymetric contours of 200, 500, 1000, 2000, 3000 m are drawn.

The upper limb of this overturn should consist of surface currents that transport waters to the northwestern shelf where DSW forms. However, our knowledge on its characteristics is still fragmentary. For example, although the East Sakhalin Current as a western boundary current in the Sea of Okhotsk has been studied by surface drifter [Ohshima et al., 2002] or mooring observation [Mizuta et al., 2003; Fukamachi et al., 2004], the other part of the surface current has not been even identified. Salinity advection processes of the upper limb are important in particular because it is salinity that determines the DSW density and subsequent ventilation characteristics. It was suggested that the surface northward currents in the eastern Sea of Okhotsk transport relatively salty water, of which salinity is influenced substantially by tidal mixing along the Kuril Islands as well as saline inflows from the North Pacific Ocean [Nakamura et al., 2006; Matsuda et al., 2009]. Several observations have indicated that the North Pacific water, advected by the East Kamchatka Current from the Bering Sea, enters the Sea of Okhotsk across the northern Kuril Straits [e.g. Stabeno et al., 1994; Ohshima et al., 2010]. Therefore, the DSW salinity may be affected by variations in the sea surface salinity (SSS) of water advected

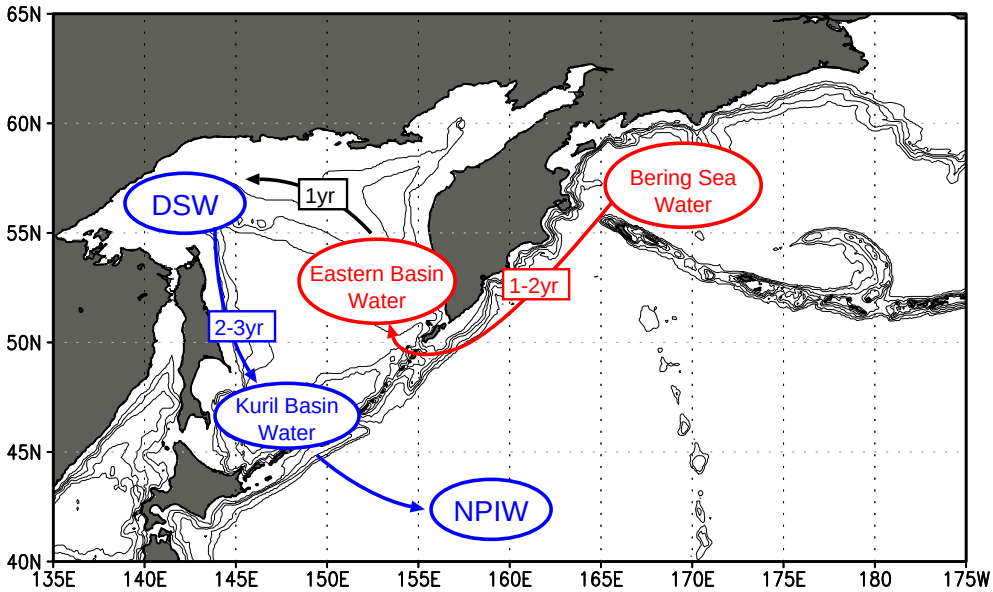

Figure 2: Image of overturning circulation with time scales from Uehara et al. [2014].

via the Bering Sea from the subarctic North Pacific [e.g. Uehara et al., 2014]. As for the water exchange between the Sea of Okhotsk and the North Pacific, the Kruzenshtern Strait and the Bussol Strait is said to be important. However, it is from the depth of the straits (the Bussol Strait and Kruzenshtern Strait are first and second deepest, respectively), but not from the mechanical consideration. Besides, the transport amount of it has not been agreed mainly because of the lack of observation [e.g., Nakamura et al., 2000; Katsumata et al., 2010].

Variations in the DSW salinity can be considered to be a cause of the variations in the intermediate layer, such as a warming trend and decadal scale variations in the Sea of Okhotsk and the North Pacific [Itoh, 2007; Nakanowatari et al., 2007]. Since the surface-forcing anomaly such as that of precipitation minus evaporation ($P - E$) will be conveyed to the intermediate layer via the DSW variations, it is important to investigate the mechanisms that induce SSS variations to understand the variability in the intermediate layer.

The previous modeling studies [e.g. Matsuda et al., 2009] found that the overturn is sensitive not only to freshwater and brine input, but also to wind stress because relatively saline water in the southern Okhotsk Sea is advected to the northwestern shelf by wind driven circulation. That is, the DSW density increases as wind stress increases, which induces intermediate layer cooling substantially by the increased cold DSW supply. In contrast, if wind ceased there would be no salty water transport to the northwestern shelf, leading to a shut down of the overturn. This is because salinity stratification, due to the high freshwater input by precipitation and riverine discharge, becomes too strong for DSW to penetrate it. This implies that the thermohaline overturn is not independent of salinity advection by wind driven circulation.

The previous models were not sufficient in resolution to discuss the salinity advection pathways [e.g. Matsuda et al., 2009]. Although Sasajima et al. [2010] achieved high resolution in the northwestern continental shelf using a curvilinear coordinate model, which is essential to represent the formation and transport of DSW by resolving eddies and coastal polynyas [e.g., Chapman and Gawarkiewicz, 1997; Kawaguchi and Mitsudera, 2009], their coordinate system

was too coarse for the southern Okhotsk Sea and the Kuril Straits to resolve the topographic features and eddies. Further, in order to represent salt advection properly, a model should resolve currents such as the East Kamchatka Current and coastal currents in the Sea of Okhotsk.

Here we study the role of salinity advection in the intermediate overturning circulation [Talley, 2003] in the Sea of Okhotsk and the North Pacific. Considering the above, we adopted a higher resolution model which resolves eddies and topography not only in the polynya areas but also in the western subarctic seas, including the Sea of Okhotsk and the Bering Sea, to represent salinity advection via narrow boundary currents and throughflows across the straits. The purpose of this study is twofold. First, we show the salt pathways connecting the surface to the intermediate layer associated with the overturning circulation with the help of tracer experiments. Second, we discuss the sensitivity of the overturning circulation to wind stress, paying attention to the roles of salinity advection in the subarctic seas. Although Matsuda et al. [2009] examined the sensitivity of the overturn to wind, their experiments were restricted to the Sea of Okhotsk. In this study we extend the discussion to the entire subarctic seas to see how its SSS responds to the wind stress changes. Therefore the model domain covers the whole North Pacific Ocean. We then describe how the wind stress and the SSS variations impact the overturning circulation.

Model configuration is described in section 2. In section 3 preliminary experiment of tidal forcing is described. In section 4 the performance of the model such as sea ice and salinity is described. In section 5, ocean circulations that constitute the overturning circulation are described with the help of tracer experiments. Sensitivity study to wind stress and fresh water flux is described in section 6 and 7, respectively, and summary of these results and discussion are in section 8.

2 Model configuration

We adopted an ice-coupled general ocean circulation model developed at the Atmosphere and Ocean Research Institute, the University of Tokyo [Hasumi, 2006]. The model can arrange general curvilinear orthogonal coordinates horizontally by using polar stereographic projection and conformal mapping. We arranged the horizontal coordinates appropriately and realized a resolution that is finer than 3km in the northwestern continental shelf in the Sea of Okhotsk, and 7km around the Kuril Islands, while it covered the North Pacific north of 30°S, Bering Sea, and the Sea of Okhotsk (Fig. 1). Vertically 7 sigma coordinate grids were arranged shallower than 35m, under which 77 level coordinate grids were assigned. Tracer advection scheme is QUICKEST/UTOPIA.

Sea ice is formulated incorporating two-category thickness representation, zero-layer thermodynamics, and dynamics with elastic-viscous-plastic rheology. Sea ice contains 5 psu salinity and during the ice formation the remainder of the salt is released to the ocean.

Ocean and sea ice were driven by atmospheric forcing calculated from Ocean Model Intercomparison Project (OMIP) Ver. 6 (http://www.omip.zmaw.de/) and monthly-mean river runoff data from Dai and Trenberth [2002]. As for bottom topography we adopted the data from the Japan Oceanographic Data Center (JODC), partly replaced by the data from Ono et al. [2006] for the area around Kashevarov Bank in the Sea of Okhotsk.

Near lateral boundary temperature and salinity were restored to the Polar Science Center Hydrographic Climatology (PHC, Steele et al. [2001]). Note that SSS was not restored except near the lateral boundary (Fig. 1a) in order to investigate the response of SSS to the atmospheric forcing. Because of the lack of restoration, SSS in the subarctic region tends to be higher than

that of observations (see Section 3). Since we found that SSS is sensitive to wind (see Section 5), wind stress magnitude was multiplied by a factor of 0.9 for the control case.

There is no lateral inflow/outflow except for the Bering Strait, where monthly data from Woodgate et al. [2005] multiplied by a factor of 0.8 (which is in the range of uncertainty) were applied.

Near the Kuril Islands and the Aleutian Islands there is vigorous diapycnal mixing [Nakamura and Awaji, 2004; Nakamura et al., 2010] by tidal flow and its internal wave breaking. The mixing supplies salt in the surface layer from the intermediate or deep layer, and then it affects DSW density [Nakamura et al., 2006]. In order to include the effect, vertical diffusivity coefficient was enhanced around the Kuril Islands and the Aleutian Islands. It was set to 10^{-2} (10^{-3}) m^2 s^{-1} at the bottom and weakened as e^{-1} by 200m upward around the Kuril Islands (the Aleutian Islands) shallower than 2000m (1800m).

Further, tidal forcing of K1 tide was given in the prognostic equation of barotropic velocity as

$$\frac{\partial \boldsymbol{v}}{\partial t} + (\boldsymbol{v} \cdot \nabla)\boldsymbol{v} + f\boldsymbol{k} \times \boldsymbol{v} = -g\boldsymbol{\nabla}(\alpha_0\eta - \beta_0\zeta) + A_H\nabla^2\boldsymbol{v},$$

$$\zeta = K \sin 2\phi \cos(\sigma t + \lambda),$$

where $\alpha_0 = 0.90, \beta_0 = 0.69$, according to Schwiderski [1980]. $K = 0.14$ m and $\sigma = 0.72921 \times 10^{-4}$ s^{-1} are amplitude and frequency of K1 partial tide respectively. ϕ denotes latitude, and λ longitude. Sea surface height at the model boundary was not specified because the boundary is far from the Sea of Okhotsk and the Bering Sea; its effects were small in these seas as shown in the Appendix. Vertical diffusivity was then estimated by the turbulent closure scheme of Noh and Kim [1999]. Vertical diffusivity coefficient was finally decided at each time step to be maximum of (1) background value of 0.13–2.91 $\times 10^{-4}$ m^2 s^{-1} which depends on the depth [Tsujino et al., 2000], (2) enhanced value around the Kuril Islands and Aleutian Islands, and (3) the value by turbulent closure of Noh and Kim [1999]. Only K1 tide was considered because vigorous mixing around the Kuril Islands is caused mainly by K1 tide [Tanaka et al., 2010]. Resultant vertical diffusion is displayed in Fig. 8.

Numerical integration started with initially no flow and no stratification. In the first year, temperature and salinity of all grids were restored to the climatology. After the second year, spinning up was done for 60 years without the restoration. The model output for the last 2 years was used for the analysis.

3 Overview description of the control run

3.1 Major currents

Major currents in the North Pacific Ocean such as the Kuroshio, Oyashio and Alaskan Stream are represented well in the model (Fig. 3). Vigorous mesoscale features are also observed. Kuroshio flows along the south coast of Japan and separates from the coast around 35°N, followed by the Kuroshio Extension. The average transport of Kuroshio measured along the ASUKA line (Fig. 3) is 29.9 Sv (Sv=10^6 m^3 s^{-1}) over 2 years, which is comparable to that estimated by mooring measurements [Imawaki et al., 2001].

The East Kamchatka Current, a western boundary current in the subarctic gyre, flows along the coastline of the Kamchatka Peninsula, from the Bering Sea to the North Pacific. It sometimes releases eddies to the western subarctic gyre. The average transport through the Kamchatka

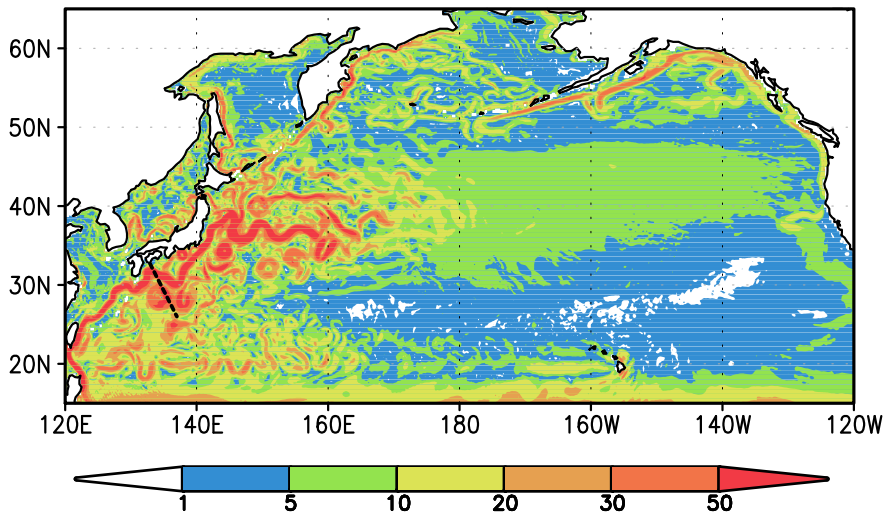

Figure 3: Sea surface speed ($\times 10^{-2}$ m s^{-1}) in December. Black short dashed line indicates the ASUKA line (from 132.9°E, 32.7°N to 137.0°E, 26.0°N).

Strait is 10.7 Sv over 2 years. The maximum speed exceeds 0.4 m s^{-1} at 55°N, which is consistent with the surface drifter observation: 0.27 m s^{-1} in average with 0.13 m s^{-1} of standard deviation in upstream region of the Kamchatka Strait (cross section 2 in Stabeno et al. [1994]).

In the Sea of Okhotsk, there is the western boundary current called as the East Sakhalin Current [e.g., Ohshima et al., 2004]. Its average transport at 53°N is 4.6 Sv over 2 years, which is comparable to but somewhat smaller than that from mooring observations (6.7 Sv by Mizuta et al. [2003]). After it passes the Cape Terpeniya at about 48°N, a part of it flows westward along the bathymetric contour of 500m, and then southward to Hokkaido Island and flows out to the North Pacific. The other part flows eastward along the bathymetric contour of 3000m of the Kuril Basin. These two paths are similar to the ones observed by the surface drifters [Ohshima et al., 2002].

3.2 Sea surface salinity (SSS)

The model represents SSS well (Fig. 4) even though it is not restored to the observation except for the areas near the lateral boundaries of the model domain (see Fig. 1). High salinity lies in the subtropical gyre and low salinity in the subarctic gyre, separated by a strong front along the gyre boundary. In the subarctic region, relatively high salinity is seen in the Bering Sea and the western gyre, although the simulated SSS is slightly higher than the observed one. The saline water also extends to the eastern part of the Sea of Okhotsk via the Kuril Islands. Low salinity in the middle and southern part of the Sea of Okhotsk is caused by sea ice melting and river runoff. Along the coasts of the subarctic seas very low salinity can be seen, which is attributed to river runoff.

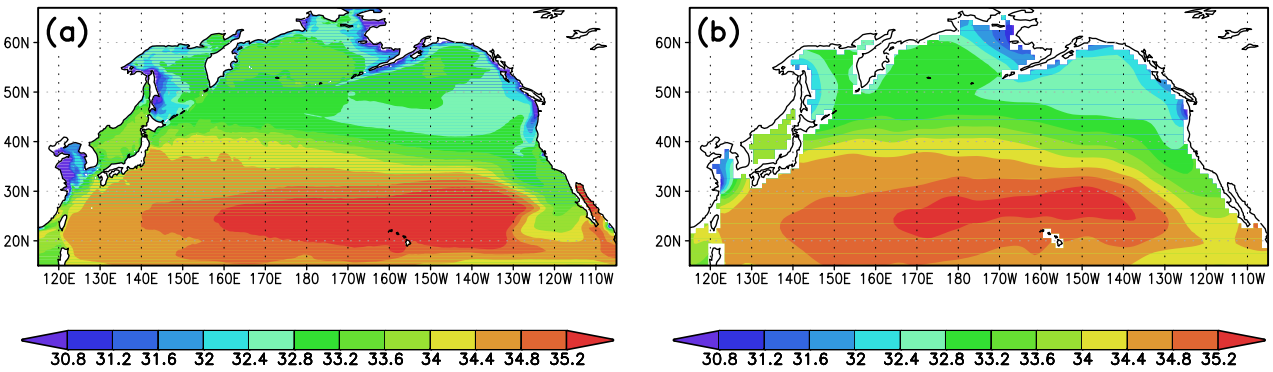

Figure 4: (a) Sea surface salinity averaged over one year in this model. (b) Same as (a) but WOA98.

3.3 Sea ice

Sea ice distribution is well represented compared with that observed from satellites (Fig. 5, also see Nihashi et al. [2009]). Total ice production in the Sea of Okhotsk during winter is 1.3×10^{12} m^3. In the Sea of Okhotsk, about one third of the ice formation occurs in the coastal polynyas in northern and northwestern continental shelves (4.5×10^{11} m^3.), while the rest occurs further offshore. This is consistent with the estimates from satellite observation (4.7×10^{11} m^3 in the northern and northwestern shelf coastal polynya regions [Nihashi et al., 2012]).

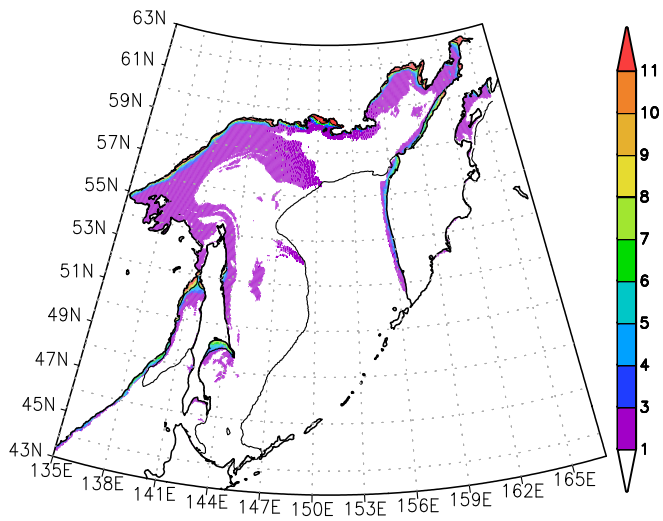

Figure 5: Ice production (m/annual) during 59/60th winter (color) and sea ice concentration of 0.7 (contour) in February.

In the Bering Sea there are coastal polynyas on the continental shelves, where sea ice is vigorously produced. Total ice production in the Bering Sea is 1.2×10^{12} m^3 during winter.

3.4 Intermediate layer

DSW is produced in the polynyas along the northern coast of the Sea of Okhotsk where sea ice production is enormous as shown in Fig. 5. DSW then flows the northwestern shelf and along the east coast of Sakhalin as seen in potential temperature on $26.85\sigma_\theta$ (=26.85 kg m^{-3}) isopycnal surface (Fig. 6a). In this layer it is cold and fresh in the western part of the Sea of Okhotsk where DSW flows, while warm and saline in the eastern part where the North Pacific water intrudes. This feature resembles that by observations [Itoh et al., 2003; Uehara et al., 2012]. Fig. 6b displays a cross section of the potential temperature and potential density at

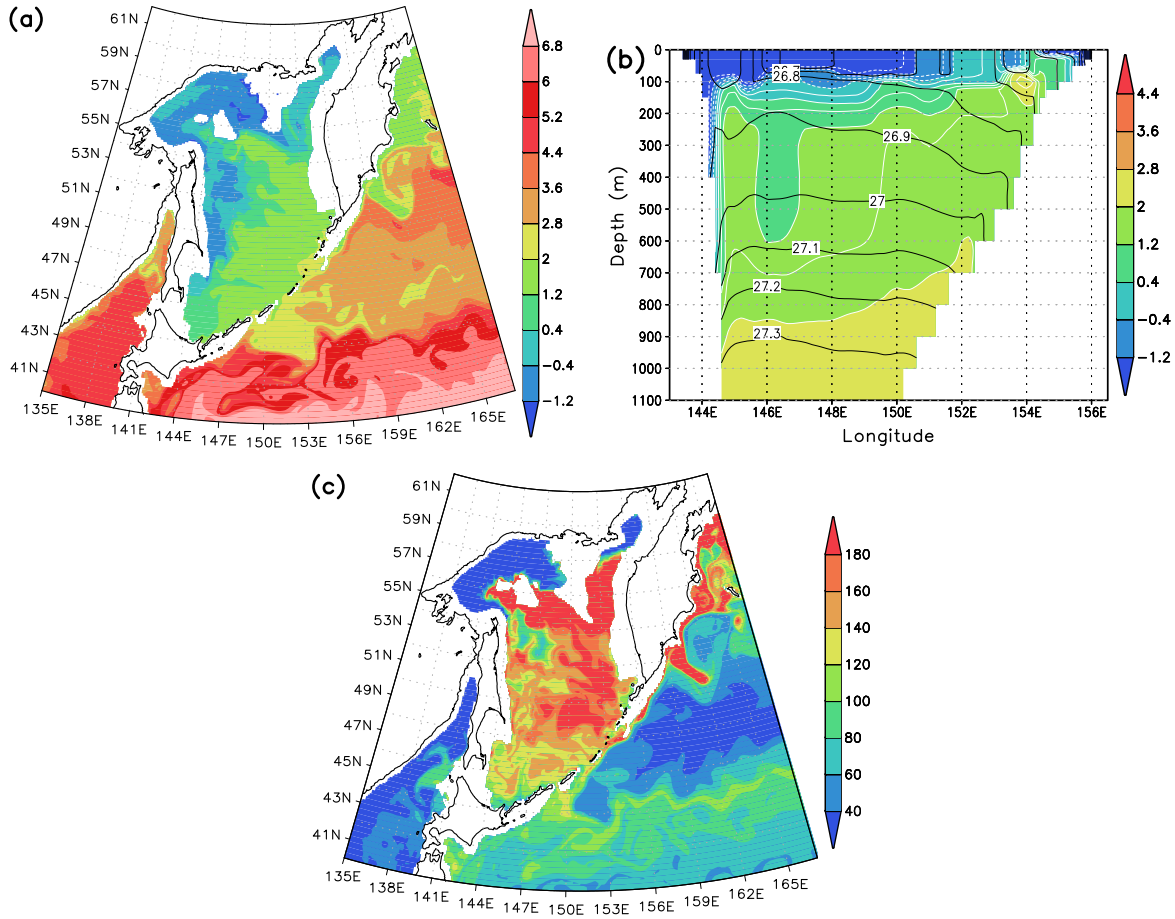

Figure 6: (a) Potential temperature on $26.85\sigma_\theta$ isopycnal surface in September. (b) Cross section of potential temperature (color) and potential density (contour, kg m^{-3}) across 53°N in February. (c) Thickness of $26.85\sigma_\theta$ isopycnal layer ($\times 10^{-1}$ m) evaluated between $26.845\sigma_\theta$ and $26.855\sigma_\theta$ isopycnal surfaces.

53°N in the Sea of Okhotsk. The cold water subducts to a depth of 700m adjacent to the western boundary. Density contours indicate that the cold water flows southward in part as a density-driven current. This must be the DSW intrusion from the northwestern coastal polynya. DSW ranges up to $27.1\sigma_\theta$ in terms of potential density.

The layer thickness of $26.85\sigma_\theta$, defined by the thickness between $26.845\sigma_\theta$ and $26.855\sigma_\theta$ isopycnal surfaces, is displayed in Fig. 6c. It can be considered as a conservative quantity when the gradient of Coriolis parameter and relative vorticity are both small. The layer thickness

distribution is also consistent with Itoh et al. [2003] and Uehara et al. [2012]; for example, it is thin in the subarctic gyre of the North Pacific, and thick in the eastern part of the Sea of Okhotsk. Further, a thick layer is present in the Kuril Basin in the southern Sea of Okhotsk. The thick and cold water flows out from the Sea of Okhotsk to the North Pacific mainly through the Etrof Strait, Urup Strait, and Bussol Strait (Fig. 1) as seen in Fig. 6a. In the North Pacific a part of the thick outflow spreads eastward along 44°N with large fluctuations, and the rest is advected southward along the Japanese coast.

There is also a thick water layer in the vicinity of the east of Kamchatka Peninsula, located inshore of the axis of the East Kamchatka Current. This near-shore water enters the Sea of Okhotsk and makes the intermediate-layer water thick in conjunction with tidal mixing at the Kuril Straits.

3.5 Effects of tidal forcing

Tidal forcing varies the distribution of SSS. Figure 7 shows the SSS anomaly in CTR relative to the case same as CTR but without tidal forcing of K1 (referred as no-tide case). The tidal forcing caused the higher SSS in the Sea of Okhotsk, the Bering Sea especially. A high salinity along the Oyashio Extension seems to be derived form the Sea of Okhotsk. Annual mean of SSS in the Sea of Okhotsk in no-tide case is 32.06psu; the tidal forcing causes anomaly of +0.23 psu in the Sea of Okhotsk. The effect is larger than that by 10% wind stress change.

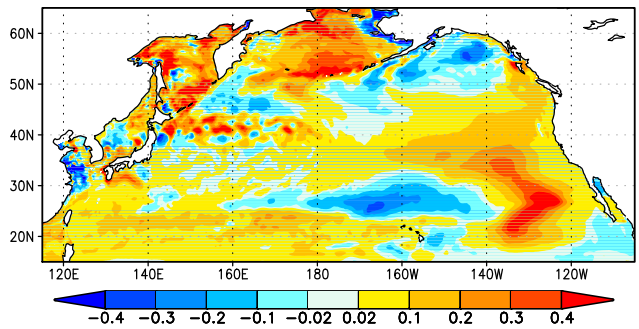

Figure 7: Annual mean SSS anomaly (psu) in CTR relative to no-tide case.

Vertical diffusion coefficients at 200m depth caused by tidal flow in CTR are shown in Fig. 8. Around the Kuril Islands and the Aleutian Islands the vertical diffusion coefficient is enhanced. On the continental shelf of the Sea of Okhotsk and the Bering Sea also high diffusion coefficients are recorded. These distributions are similar to that by Nakamura et al. [2004] and Foreman et al. [2006]. Considering above, we can say the reasons why SSS in the Sea of Okhotsk become higher by tidal forcing are the vertical mixing along the Kuril Islands and continental slopes and enhanced water exchange between the Sea of Okhotsk and the North Pacific.

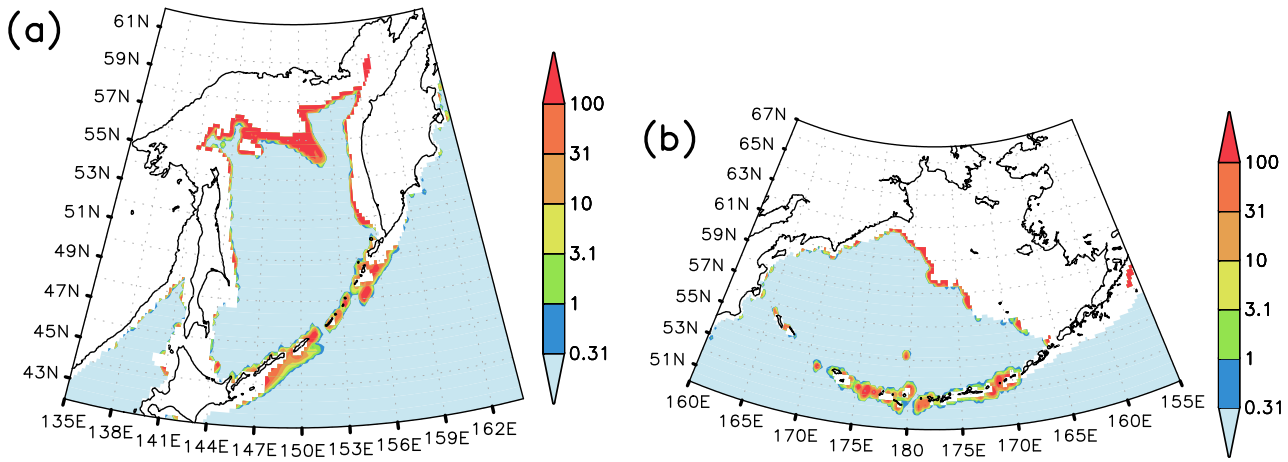

Figure 8: Vertical diffusion coefficients ($\times 10^{-4}$ m^2 s^{-1}) at a depth of 200 m in September in CTR.

4 Three dimensional structure associated with the Sea of Okhotsk-North Pacific overturning circulation—Tracer experiments

It was hypothesized that the relatively saline water intrudes into the Sea of Okhotsk from the North Pacific and becomes a source water of DSW [e.g. Ohshima et al., 2010]. In this subsection we describe the surface saline water pathway that carries the North Pacific water to the northwestern shelf where DSW forms.

In order to represent surface salt pathways, tracer experiments were carried out. In each experiment a passive tracer was put into the uppermost layer, where tracer concentration was kept at unity in a specified area. It was then advected by background currents and was not taken up by sea ice. Numerical integration started from the 61st year of the control run.

4.1 Surface pathways in the Sea of Okhotsk

At first, we put a tracer into an area to the west of the Kamchatka Peninsula (the rectangular area of Fig. 9a) from 1st January. Distribution of the tracer in February of the second year, at 14 months after the tracer was released, is shown in Fig. 9a. Tracer is advected via two pathways. One is a northward current along the western coast of the Kamchatka Peninsula, followed by a westward current along the northern coast of the Sea of Okhotsk. In order to reach the coastal polynyas over the northwestern shelf, the tracer should be carried by these currents. The other is a westward current associated with the cyclonic circulation along the bathymetric contours deeper than 500m. It finally connects the East Sakhalin Current. However, this route never passes the coastal polynya area over the northwestern shelves.

4.2 Bering-Okhotsk connection via East Kamchatka Current

Next, tracer was input in the western continental shelf of the Bering Sea to the north of 62°N. It was advected to the Sea of Okhotsk via the East Kamchatka Current (Fig. 10a). Tracer

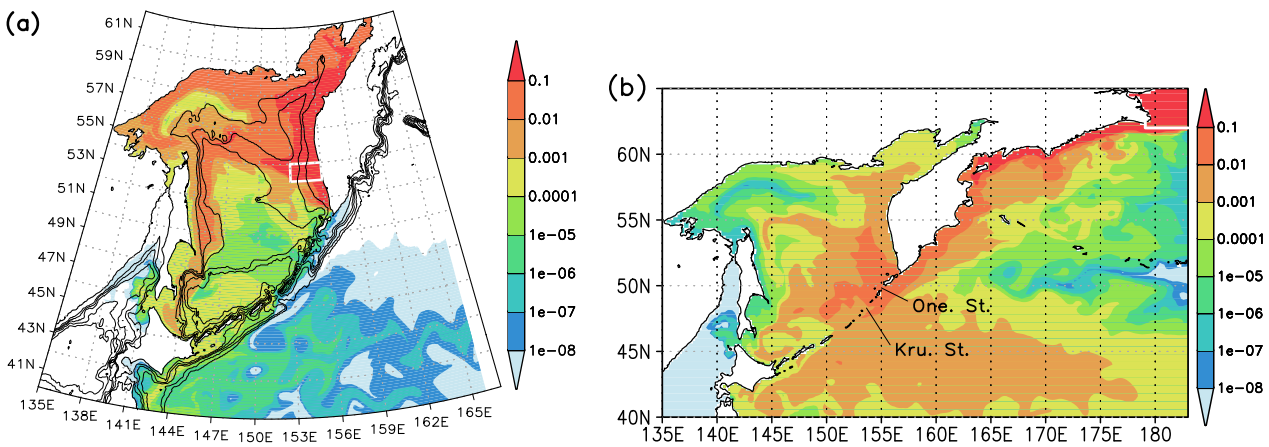

Figure 9: (a) Tracer concentration at the sea surface in February of the second year. White rectangular denotes where the tracer was input. (b) Tracer concentration at the sea surface of another experiment, in February of the third year. Tracer was input north of the white line.

flows from the northern part of the Bering Sea adjacent to the east coast along the Kamchatka Peninsula. This must be the salinity advection route from the Bering Sea to the Sea of Okhotsk. With a closer look at the thickness in the intermediate layer (Fig. 6b) and SSS (Fig. 4), we note that the East Kamchatka Current has an inshore branch with low potential vorticity and relatively low SSS water collocated with this tracer pathway.

After the tracer reaches the Kuril Islands, it enters the Sea of Okhotsk in winter, while it is advected southwestward along the Kuril Island with only slight inflow into the Sea of Okhotsk in summer and autumn. Tracer enters from northern Kuril Straits including the Kruzenshtern Strait and the Onekotan Strait.

Figure 9b represents the tracer distribution at 2 years and 2 months after the tracer was released. Considering that the West Kamchatka Current and the Northern Coastal Current advects the tracer from the eastern basin subsequently, advection time scale from the Bering Sea to the DSW formation region is estimated to be 2–3 years.

4.3 Surface currents toward the DSW formation region in the Sea of Okhotsk

In order to see velocity field visualized by the tracer, we display a surface current field in the eastern basin of the Sea of Okhotsk in Figure 10a. As for the throughflows across the Kuril straits, the Onekotan Strait has a net throughflow into the Sea of Okhotsk with a regular seasonal variation (Fig. 10c). The inflow transport becomes as large as 0.8 Sv in February and the surface velocity exceeds 0.1 m s^{-1}, connecting to the West Kamchatka Current (Fig. 10a). There is some evidence for the Onekotan throughflow such as drifter tracks [Stabeno et al., 1994] and SST distribution [Kurashina et al., 1967; Talley and Nagata, 1995]. This seems reasonable because the Onekotan Strait is the northernmost deep strait (∼500m), so that coastally trapped waves generated along the North Pacific rim during winter [Tsujino et al., 2008] encounter this strait and can propagate through this strait (see also Fig. 10d). In contrast, although the inflow through the Kruzenshtern Strait is large (3.5 Sv in annual mean), it does not tend to go northward but westward to the Kuril Basin.

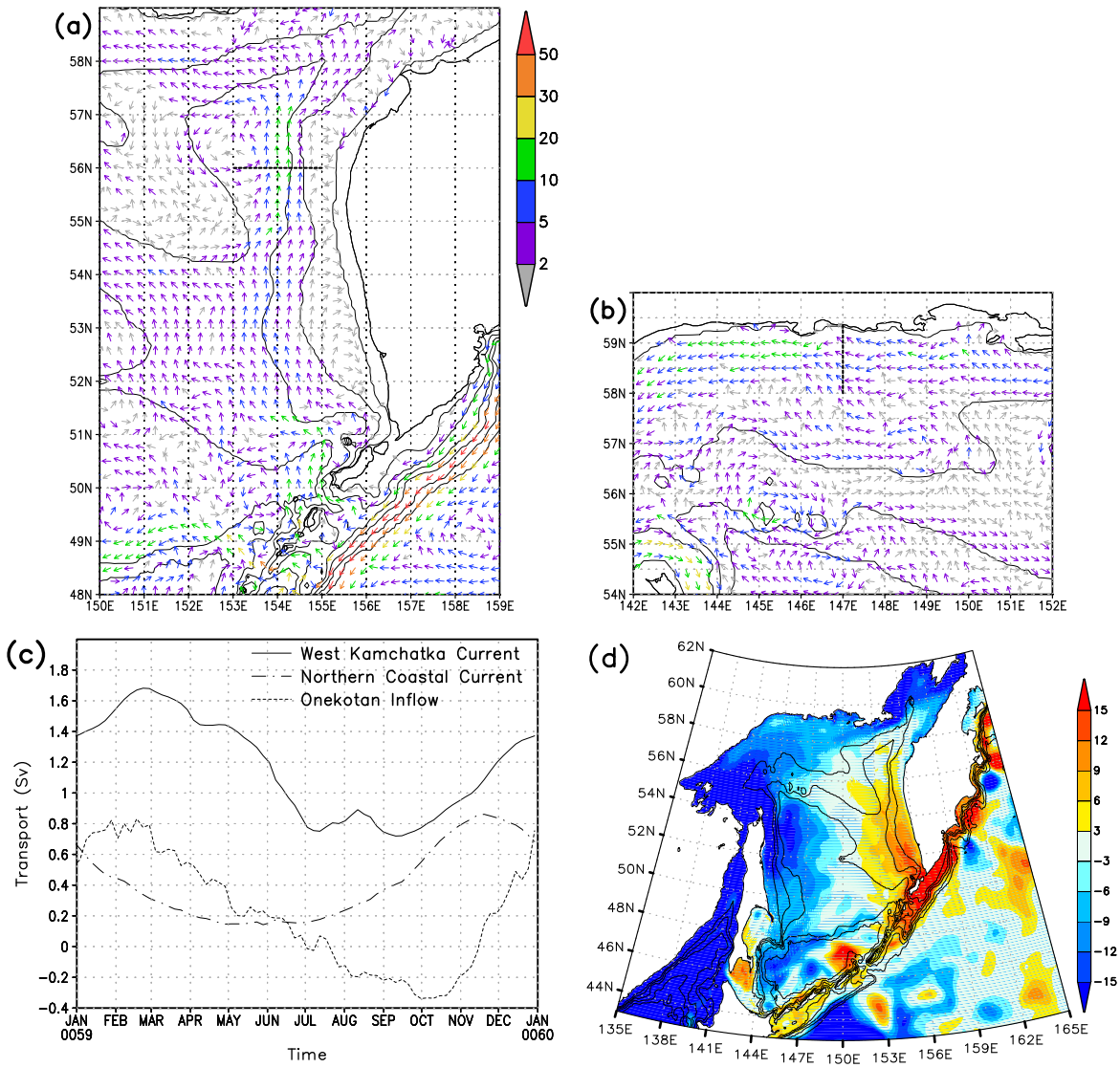

Figure 10: (a) Current offshore of the Kamchatka Peninsula in February. Red, orange, yellow, green, blue, purple and gray arrows indicate speed over 50, 30–50, 20–30, 10–20, 10–5, 5–2 $\times 10^{-2}$ m s^{-1} and less than 2 $\times 10^{-2}$ m s^{-1}, respectively. Bathymetric contours of 50, 200, 500, 1000, 2000, 3000 m are drawn. (b) Same as (a) but in the northern shelf in November. Black short lines in (a) and (b) indicate the measurement lines along which the transports of the West Kamchatka Current and the Northern Coastal Current were evaluated, respectively. (c) Transport of the West Kamchatka Current at 56°N (solid line) and Northern Coastal Current at 147°E (dot-dashed line). They were measured along the lines depicted in (a) and (b). Inflow through the Onekotan Strait is also shown (short dashed line. Negative value means outflow). (d) Sea surface height anomaly ($\times 10^{-2}$ m) in February relative to August.

Throughflows of the Kuril straits in the each case are plotted in Fig. 11. In only-tide case (see Appendix A) it records net inflow of 0.20 Sv through the Kruzenshtern Strait and outflow of 0.23 Sv through the Bussol Strait, although there is sometimes bi-directional flow in the

Kruzenshtern Strait. In Fig. 11 the throughflows in CTR and no tidal forcing experiment in which other conditions except for tidal forcing are the same as CTR (no-tide case) are also shown. In the Onekotan Strait the throughflow in CTR can be considered as the sum of that in only-tide case and no-tide case. Interestingly, however, the throughflows of the Kruzenshtern Strait and the Bussol strait are much larger than those expected by only-tide case and no-tide case. Highly nonlinear effect or something important must occur, but it is not studied here.

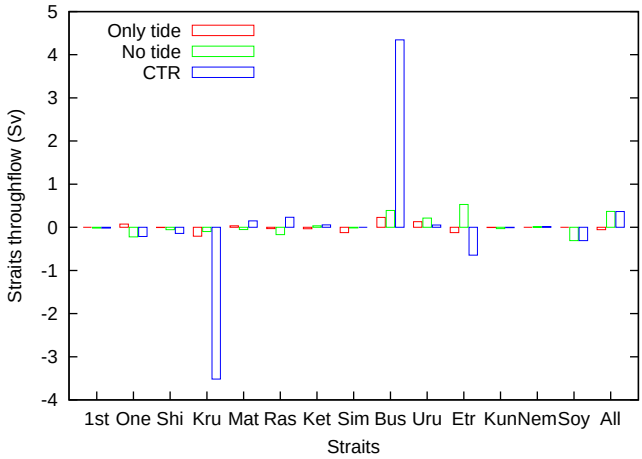

Figure 11: Throughflow of each straits (Sv). Positive values mean the outflow, and negative mean inflow. Red, green and blue boxes denote the only-tide case, no-tide case, and CTR. Abbreviation of straits in the Kuril straits here denote below: 1st Kuril Strait, Onekotan Strait, Shiashikotan Strait, Kruzenshtern Strait, Matua Strait, Rasshua Strait, Ketoy Strait, Simushir Strait, Bussol Strait, Urup Strait, Etrof Strait, Kunashiri Strait, Nemuro Strait. Soya Strait between the Sakhalin Island and the Hokkaido Island and the total of Kuril straits are also shown.

The water from Onekotan Strait flows northward, which then bifurcates into a northwestward current and a northward current at about 54°N as seen in the tracer experiment. The northward current is located along the west coast of the Kamchatka Peninsula along the contour at 500m deep and is strengthened at 55–57°N. We call this northward current "the West Kamchatka Current".

The West Kamchatka Current has a large seasonal variability; it is strong in winter where its transport maximum is 1.7 Sv at 56°N in February (Fig. 10c), and the velocity maximum exceeds 0.16 m s^{-1}. Its seasonal variability is characterized by the sea surface height (SSH) anomaly in winter relative to that in summer (Fig. 10d). The SSH anomaly extends from the east coast of the Kamchatka Peninsula to the eastern part of the Sea of Okhotsk via the northern Kuril Straits, consistent with for example Tsujino et al. [2008] and Ohshima et al. [2010]. Note that in winter the West Kamchatka Current flows in the opposite direction to the local northerly wind, implying that this is a current associated with coastally trapped waves generated remotely along the northwestern rim of the North Pacific Ocean.

Another notable current that advects the tracer, following the West Kamchatka Current, is a westward current along the northern coast as shown in Fig. 10b. We call this the "Northern Coastal Current". It appears in September, and becomes wider gradually with a maximum transport of ∼0.9 Sv in November (Fig. 10c). The seasonal variation is similar to the coastal

current measurement by Shcherbina et al. [2003]. It advects the tracer in autumn, followed by advection via the West Kamchatka Current from the eastern basin in the preceding winter. This implies that it takes about one year from the eastern basin to the northwestern shelf of the Sea of Okhotsk and pre-conditions the DSW salinity.

4.4 DSW subduction and intermediate-layer pathways

In order to investigate ventilation and the following intermediate-layer pathways, we put tracer into the surface layer of the polynyas over the northwestern continental shelf (west of 143°E) when and where the ice production rate was larger than 3m per month (from the end of November to the middle of March). The area was restricted to the vicinity of the coast as a result (Fig. 5); this corresponds to the polynyas where the DSW forms.

Although the tracer was put at the surface, it was mixed to the bottom over the shallow shelf because of strong vertical mixing due to cold and saline brine rejection in the polynyas. The tracer is advected first by the Northern Coastal Current and then advected southward by the East Sakhalin Current in both the surface and the intermediate layer (Fig. 12). In the surface layer, after it reaches the Cape Terpeniya, a part of it is advected to Hokkaido Island, while the rest is advected westward and then turns southeastward across the Kuril Basin, and finally spills out mainly through the Bussol Strait, consistent with Ohshima et al. [2002].

In the intermediate layer, the tracer represents the DSW flow (Fig. 12b), corresponding to the low temperature water in Fig. 6b. It takes about 1 year for the tracer to reach the Bussol Strait in the intermediate layer of $27.0\sigma_\theta$. Compared to the surface layer, there is a larger tracer concentration in the Kuril Basin in the intermediate layer, while a low tracer concentration in the northern and central Sea of Okhotsk. This is consistent with the fact that materials such as iron have local maxima in the intermediate layer in the Kuril Basin [Nishioka et al., 2013].

A cross section at 53°N of the tracer concentration shows two components of the East Sakhalin Current; one is in the surface layer located west of 144°E, the other is in the intermediate layer of 200–700m in depth, 26.9–$27.0\sigma_\theta$ in potential density (Fig. 12c). The intermediate-layer component of the East Sakhalin Current has a larger thickness than adjacent waters, exhibiting the intrusion of DSW into this layer. In spring the velocity exceeded 0.15 m s^{-1} with a local maximum in the intermediate layer. This implies that the East Sakhalin Current has a density-driven component due to DSW intrusion as well as a wind-driven component.

Figure 13 displays how the tracer is distributed in the temperature-salinity (T/S) plane. In this figure tracer total amount was shown; that is, concentration is multiplied by volume of each grid and this was integrated in the Sea of Okhotsk. In the T/S histogram the tracer that is put initially in the polynya over the northwestern shelf starts at freezing point in the density ranging between $26.5\sigma_\theta$ and $26.8\sigma_\theta$ in December (Fig. 13a). It gradually becomes denser by brine rejection and reaches 26.8–$27.0\sigma_\theta$ in February (Fig. 13b). In March and afterwards, the tracer moves to warmer water without significant density change (Fig. 13c). This represents southward advection of cold DSW in the intermediate layer and isopycnal mixing with surrounding warmer waters. Two years after the tracer was input (Fig. 13d), a local maximum of the tracer concentration at 1 °C on $26.95\sigma_\theta$ appears. The tracer corresponding to the maximum is located in the central part of the Okhotsk Sea. During the mixing process, the tracer distribution in the T/S histogram moves to denser a little. Other than diapycnal mixing, cabbeling effect can be considered. Assuming that the water in freezing point continues to mix with the water of same density and 2 °C, its density, which is initially $27.00\sigma_\theta$, can become $27.05\sigma_\theta$.

Figure 14 shows the time series of tracer volume ratio in the Kuril Basin, that is, tracer

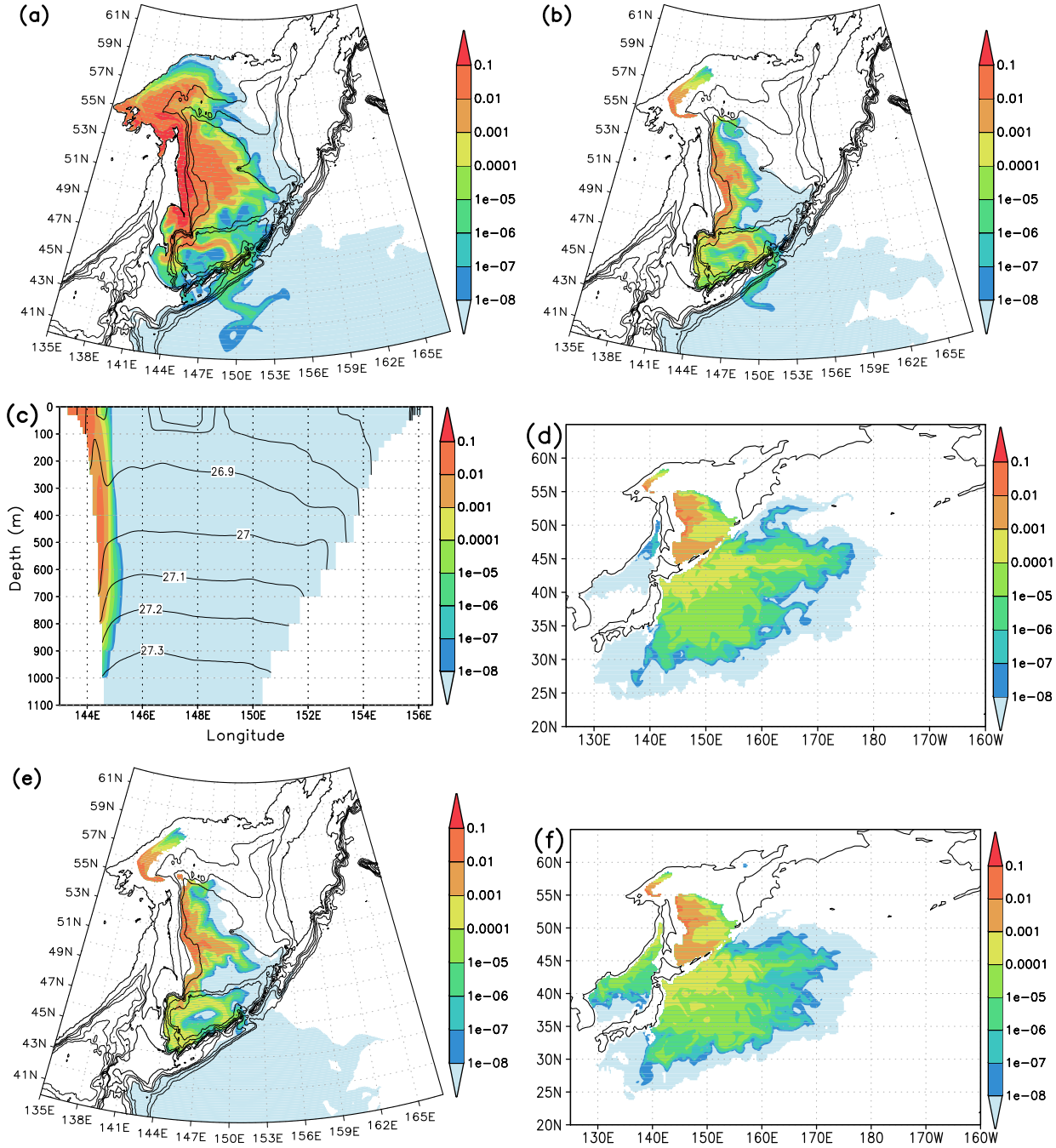

Figure 12: (a) Tracer concentration in the surface layer in October of the second year after tracer was input. The tracer started in the surface layer of the coastal polynya over the northwestern continental shelf. (b) same as (a) but on the $27.0\sigma_\theta$ isopycnal surface. (c) Tracer concentration across 53°N and potential density (contour) in April of the second year. (d) Tracer concentration on the $27.0\sigma_\theta$ isopycnal surface in October of the third year. (e) and (f) same as (b) and (d) but in the experiment in which tracer was input from year 64 (3 years after the former experiment).

concentration multiplied by volume of each grid and integrated in the Kuril Basin, and then normalized by the volume of the Kuril Basin itself. Although tracer reaches the Kuril Basin

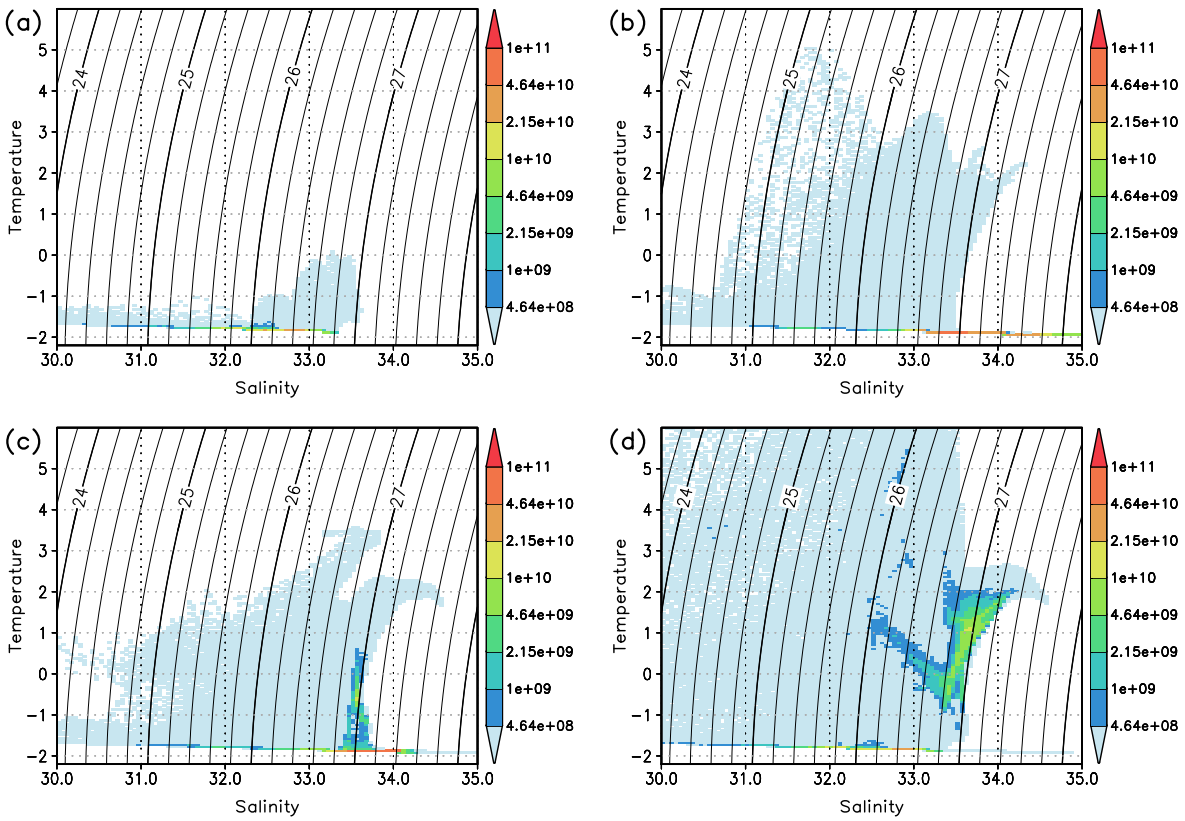

Figure 13: Temperature-salinity histogram of tracer volume (concentration multiplied by volume in each grid) in (a) December of the first year, (b) February of the second year, (c) April of the second year, (d) December of the third year.

within a year, the tracer volume in the Kuril Basin continues growing for another half year. Besides, the tracer input in the second-year winter also has a substantial impact on the tracer-volume increase in the Kuril Basin, so it takes about 2–2.5 year to connect the northwestern continental shelf and the Kuril Basin. This is consistent with Uehara et al. [2014] which showed that potential temperature in the Kuril Basin is correlated with the DSW salinity anomaly with a lag of a few years.

After the tracer outflows to the North Pacific, it spreads widely in the intermediate layer (Fig. 12d). Some propagates eastward along the Oyashio front and other spreads southward across the Kuroshio Extension, both are accompanied by many eddies. The southward advection ventilates the NPIW in the subtropical gyre. There is also a northward stretch from subarctic gyre to the Bering Sea around 160–170°E.

Figure 12e and 12f are the same as Fig. 12b and 12d, respectively, but a different tracer experiment in which tracer was input from year 64 (3 years after the former experiment). We can see the distributions of the tracer are similar; that is, the pathway of the intermediate layer limb of the overturning circulation is robust, as well as the timescale, although there are many eddies in the Kuril Basin. Tracer volume ratio in the Kuril Basin is also similar in the two cases, but there is little annual fluctuation in the tracer volume ratio (Fig. 14). This is due to the fluctuation of the East Sakhalin Current. For example, in year 68 (corresponding year 65 for red line) the transport of East Sakhalin Current is larger and then the tracer volume ratio grows

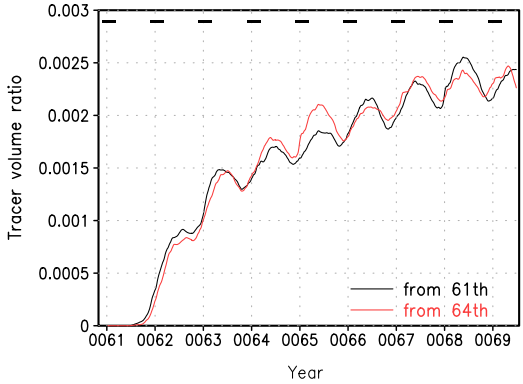

Figure 14: Time series of tracer volume ratio in Kuril Basin normalized by the volume of the Kuril Basin. Kuril Basin was defined as the region deeper than 2000m in the southern part of the Sea of Okhotsk. Black and red lines are in the case that tracer was input from year 61th and year 64th, respectively. The red line is shifted for 3 years and drawn. The black bars denote the periods of tracer input.

more, on the other hand, in year 65 (62 for red line) the transport is small, tracer volume grows less.

4.5 Brief summary of the tracer experiments

The three experiments of tracer revealed the pathways and time scales of overturning circulation. Tracer is advected from the Bering Sea by the East Kamchatka Current, the throughflow across the Kuril Straits, the West Kamchatka Current, the Northern Coastal Current and reaches the DSW formation area. Subsequently, DSW subducts to the intermediate-layer branch of the East Sakhalin Current (Fig. 15). In particular, the low potential vorticity water inshore of the East Kamchatka Current, which flows through the Onekotan Strait in winter, is an important source water for DSW. It takes about 1–2 years to be advected from the Bering Sea to the eastern basin in the Sea of Okhotsk. The West Kamchatka Current and the Northern Coastal Current are strong from January to March and from September to November, respectively. There is a seasonal period of slow flow in summer, and as a result, it takes about 1 year to be advected from the eastern basin to the northwestern continental shelf. Subsequently, DSW intrudes to the intermediate layer by gaining potential density up to $27.1\sigma_\theta$. DSW flows in the intermediate layer isopycnally which composes the lower component of the East Sakhalin Current. DSW which starts in January reaches the Bussol Strait in 10 months, but it takes 2–3 years to fill the Kuril Basin (Fig. 14). The Kuril Basin water derived from DSW flows out and spreads to the North Pacific Ocean, ventilating the NPIW. These features are summarized in Fig. 15, and the time scales are consistent with those from data analyses by Uehara et al. [2014].

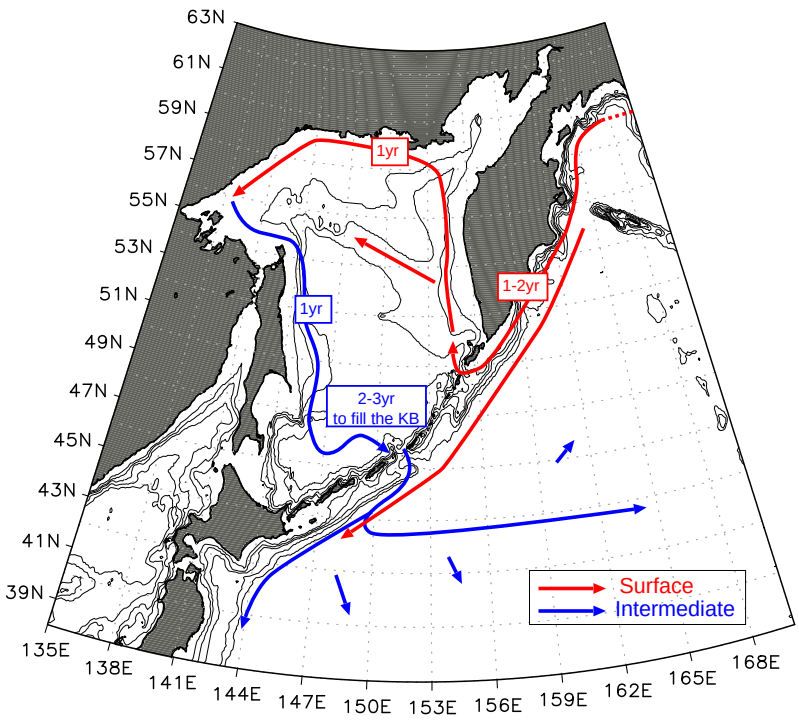

Figure 15: Schematic view of the overturning circulation in and around the Sea of Okhotsk represented by this study. Red lines indicate the current in the surface layer, and blue lines in the intermediate layer. The North Pacific water in the East Kamchatka Current enters through the Onekotan Strait, and is advected along the bathymetric contour of 500m to the northern continental shelf. DSW flows the east of the Sakhalin Island and exits through the Bussol Strait, and then spreads over the North Pacific and forms the North Pacific Intermediate Water. It takes about 1 or 2 years from the Bering Sea to the eastern basin in the Sea of Okhotsk. It takes about 1 year from the eastern basin to the northwestern continental shelf where sea ice is vigorously formed. It takes about 1 year from the northwestern continental shelf to the Bussol Strait, while it takes 2 or 3 years for the DSW to fill the Kuril Basin. The time scales were defined the time for 1 % of tracer concentration to get to.

5 Sensitivity of DSW properties and overturn characteristics to wind stress

In order to study the role of the salinity advection, sensitivity of the overturning circulation and water properties to wind stress was examined. We set wind stress using data from OMIP, multiplied by factor 0.5, 0.8, 0.9 (control), 1.0 and 1.5, which are referred to as WND0.5, WND0.8, CTR, WND1.0, and WND1.5, respectively. In each case the model was integrated for 40 years and last 2-year results were analyzed. Only the magnitude of wind stress was changed in each case; the direction of wind stress and wind speed to calculate the heat flux at sea surface by bulk formula were retained the same in all cases. Turbulent kinetic energy flux from sea surface depends on the wind stress to the power of 1.5 in the turbulent closure of Noh and Kim [1999].

In reality wind stress can change by a factor of 2 between weak-wind years and strong-wind years [e.g. Sugimoto and Hanawa, 2009]. Therefore this parameter range might not be so

unrealistic, although they are the composites of extreme years.

5.1 Sea ice production

Sea ice production in the Sea of Okhotsk was plotted vs wind stress magnitude (Fig. 16a). As wind stress is intensified, ice production increases, although it is not proportional to wind stress; ice production in the northwestern shelf and northern shelf increases by a factor of 1.1 when wind stress increases by 1.5. It is because cooling forcings such as air temperature and wind speed are the same, while the area of polynyas increases with increased wind stress, as discussed in Sasajima et al. [2010]. In fact, the ice production depends linearly on the area of polynyas as in Fig. 16b.

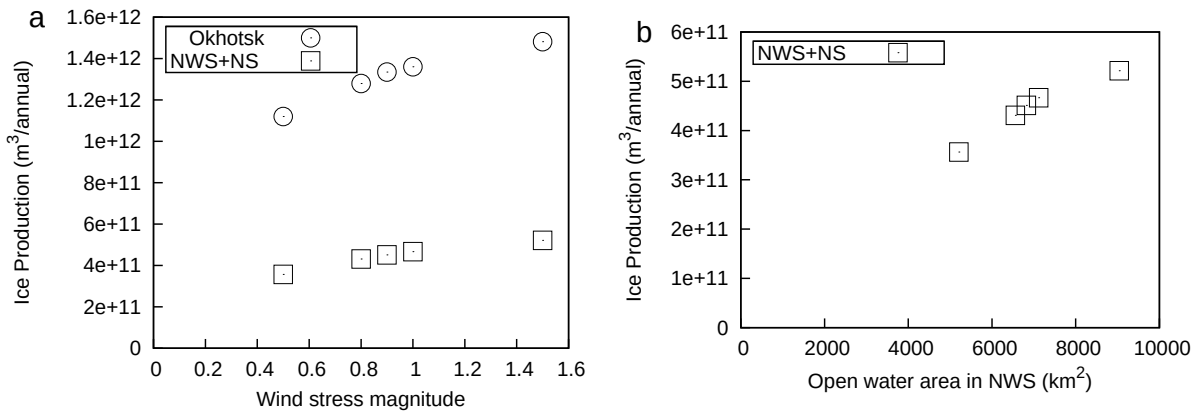

Figure 16: (a) Ice production (m^3/annual) in the northwestern shelf and the northern shelf (squares), and whole of the Sea of Okhotsk (circles) vs wind stress magnitude ratio. (b) Ice production in 1 year vs open water area in January. Both are summed over the northwestern shelf and northern shelf.

5.2 DSW production from a point of view of water mass properties

In this and next subsections, we examined the overturning transport in two ways. In this section we evaluated it by calculating the DSW production rate in which DSW was defined by temperature and density criteria. This is a conventional view with respect to DSW definition. In previous studies, DSW was often defined as the water denser than $26.6\sigma_\theta$ and colder than -1.0 °C [Gladyshev et al., 2000; Nakamura et al., 2006; Matsuda et al., 2009]. However, this definition is inadequate because the water denser than $26.6\sigma_\theta$ includes mixed layer water (cf. Fig. 6b). Further, since the DSW density, salinity, and freezing point can vary in the present sensitivity study, the thresholds of temperature and density should be defined according to each case. Sasajima et al. [2010] defined DSW as the water denser than the densest water in autumn to overcome the above problem. However, since a part of DSW may stay over on the continental shelf through the summer, newly formed water mass which is lighter than the old DSW is not considered in this definition.

Figure 17 shows temperature-salinity histogram of the water volume in the Sea of Okhotsk. From November to December (Fig. 17a, b), some waters are cooled and locate at the temperature of freezing, T_f, which depends on salinity as $T_f = 0.0543S$, where S is salinity. The water near

the freezing point has a local maximum around 26.6–26.8σ_θ in the histogram. Then, the water near the freezing point gets denser by brine rejection, and its local maximum become denser (Fig. 17c), reaches 26.8–27.0σ_θ in April (Fig. 17d). At the same time when the local maximum moves denser, a water mass moves to warmer in the histogram isopycnally around 26.85σ_θ. This corresponds to the southward flow of DSW and its mixing with surrounding waters. These features are consistent with the histogram of tracer distribution (Fig. 13) in the previous section. It also suggests that DSW can be defined as the local maximum of the water volume near the freezing point.

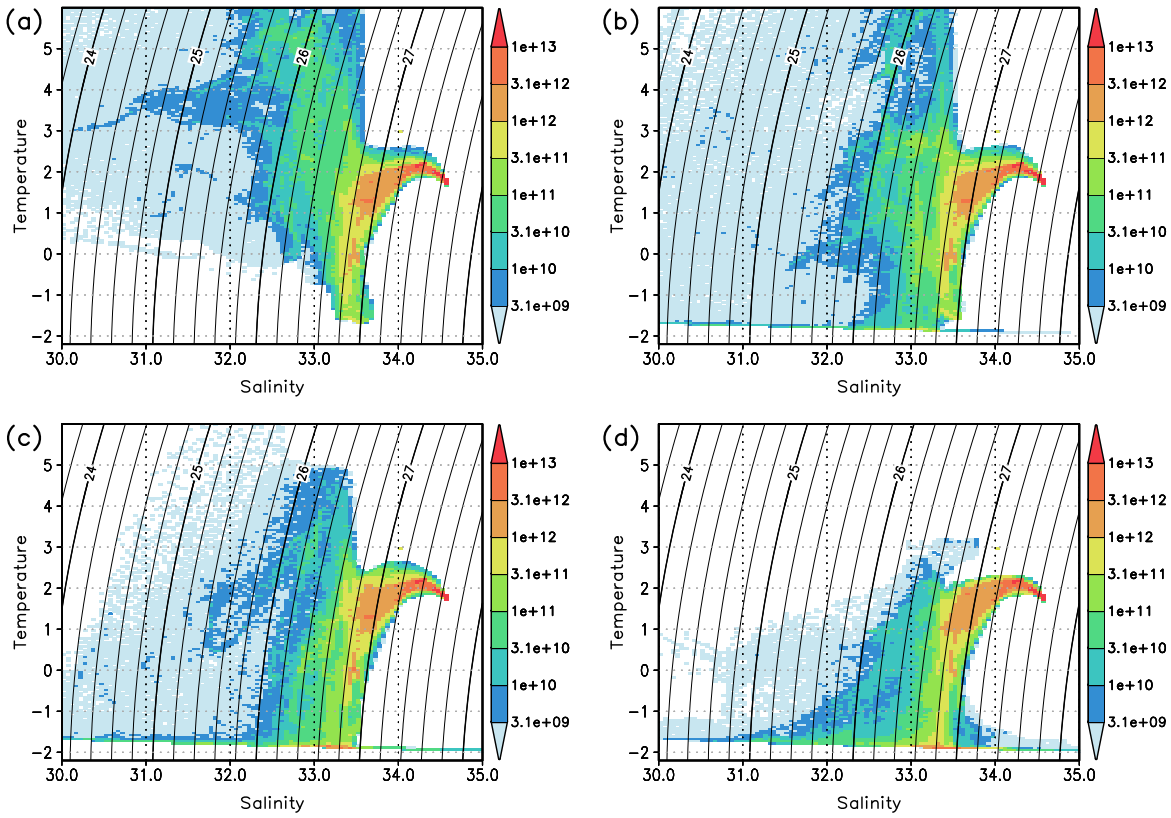

Figure 17: Temperature-salinity histogram of the water volume in the Sea of Okhotsk. (a) November, (b) December, (c) January, (d) April of 59-60th winter.

Considering the above, we defined DSW as follows. First, we adopted the water colder than a critical temperature T_c in the Sea of Okhotsk, where T_c =(*freezing temperature*)+1.0 °C. For example, if salinity is 33.0 psu, T_c is −0.79 °C since the freezing temperature is −1.79 °C. Next, we considered the density thresholds. The histogram of the water volume, in terms of density, consists of two peaks chiefly in CTR (Fig. 18), corresponding to the two types of mode waters. One has the maximum volume on a density of 26.84σ_θ, which does not change throughout a year. Therefore, this corresponds to the mixed-layer water formed in winter, and retains during other seasons as the dichothermal water [Uehara et al., 2012]. As for the denser mode water, the peak density increases during winter from 26.90–26.91σ_θ in February to 26.96–26.97σ_θ in April. Besides, it is this mode water that corresponds to the water existing over the northern shelf shallower than 200m (lines with shade in Fig. 18). Thus we define the volume relating to the denser mode water as the volume of DSW. The low-density threshold of DSW is defined

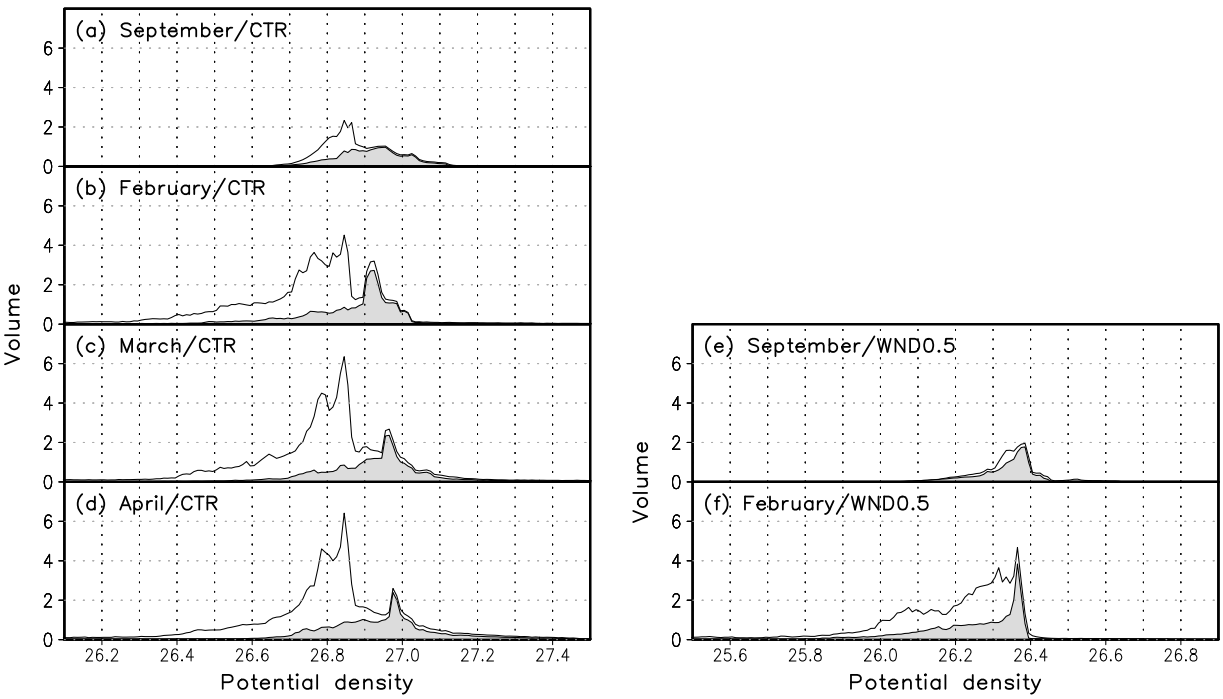

Figure 18: Volume ($\times 10^{12}$ m^3) of water colder than T_C in the Sea of Okhotsk (lines) and shelf areas (lines with shade) in (a) September, (b) February, (c) March, (d) April in CTR, (e) September, (f) February in WND0.5. Shelf here is defined as the area shallower than 200m, the west of 155°E (mouth of the Shelikhov Bay) and the north of 44.8°N (Cape Terpeniya).

by the density between the two peaks, where the volume of the lighter mode water abruptly decreases in the April histogram. For example, the threshold density is $26.87\sigma_\theta$ in CTR. The high-density threshold is defined as the density where the volume becomes e^{-2} of the peak volume. By summing up the volume of waters within the temperature and density criteria, the DSW volume was evaluated. The DSW production in a year was then defined as the difference between the maximum and minimum of DSW volume. In the control case DSW production is $(2.4 \pm 0.5) \times 10^{13}$ m^3 in a year (2.2 ± 0.5 Sv in average over a winter), which is comparable to that by Sasajima et al. [2010] within the error derived from arbitrariness of peak separation.

The DSW production defined above and its maximum density in a year were calculated for each case. We found that DSW production defined from a point of view of the water mass properties is not sensitive to wind stress variations (Fig. 19). Its insensitivity is due to invariability of cooling forcing, as was seen in case of ice production. Nevertheless, the DSW production increases slightly with wind strength; it increased by a factor of 1.1 ± 0.3 when wind stress increased by 1.5, because ice production increases slightly owing to the increased open water area (Fig. 16b; see also Sasajima et al., 2010).

As for WND0.5, surface salinity is so low. In this case the mixed layer water and DSW are not distinguishable as in Fig. 18e and 18f, and therefore, the DSW production in this case is not plotted in Fig. 19. This means that dense water produced over the shelf remains in the mixed layer, so that it cannot intrude into the intermediate layer. That is, the ventilation was shut down due to intensified stratification associated with decreased saline water supply from the North Pacific in WND0.5, consistent with Matsuda et al. [2009].

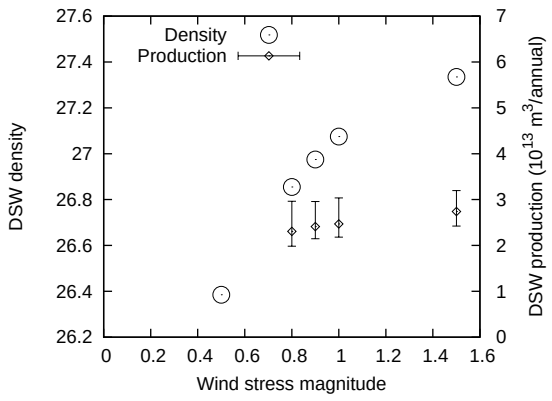

Figure 19: Maximum DSW density (σ_θ) and DSW production (m^3/annual) in 1 year vs wind stress magnitude ratio. The low-density thresholds to integrate the volume are $26.78\sigma_\theta$, $26.87\sigma_\theta$, $26.93\sigma_\theta$ and $27.19\sigma_\theta$ in WND0.8, CTR, WND1.0 and WND1.5, respectively. The error bars in the DSW production were made by the values which the DSW production becomes if the low-density thresholds moved with $\pm 0.02\sigma_\theta$ in each case. For example, the upper/lower bar in CTR is the DSW production if low-density threshold is $26.85\sigma_\theta/26.89\sigma_\theta$.

The density of the peak volume was defined as the density of DSW; $26.96\sigma_\theta$ in March in CTR. It is sensitive to wind stress (circles in Fig. 19). This is likely caused by the SSS variations in the entire subarctic seas. This will be discussed in the subsection 5.4.

5.3 Currents and diapycnal transport associated with the overturn

Another important factor that determines the DSW transport is volume flux by ocean currents [Chapman and Gawarkiewicz, 1997; Kawaguchi and Mitsudera, 2009; Matsuda et al.,2009]. We thus evaluate the overturning transport by calculating the meridional streamfunction in the Sea of Okhotsk in this subsection, which includes the effects of the current transport and its variations.

The western boundary currents are sensitive to wind as expected. The East Kamchatka Current, measured at the Kamchatka Strait (Fig. 1), increases for intensified wind (Fig. 20a). Transport of the Kuroshio measured at the ASUKA line is also proportional to wind stress (Fig. 20b), consistent with the discussion of Bryden and Imawaki [2001].

In the Sea of Okhotsk, transports of the West Kamchatka Current and the Northern Coastal Current are also proportional to wind stress in general (Fig. 20c). Therefore, these currents are mainly wind-driven. In WND0.5, transport of the West Kamchatka Current is large; more water flows the northward along the West Kamchatka Current than that in WND0.8 and CTR at the bifurcation around 54°N (Fig. 10a), although we have not identified the reasons. Figure 20d shows the transport of the East Sakhalin Current. It displays that the intensified wind brings about large transport. However, weakened wind does not cause a linear decrease in transport. This suggests that it includes a density-driven component as in Fig. 12c.

Next, in order to view the diapycnal overturn from the surface layer to the intermediate layer explicitly, we display the meridional streamfunction in density coordinates in the Sea of Okhotsk

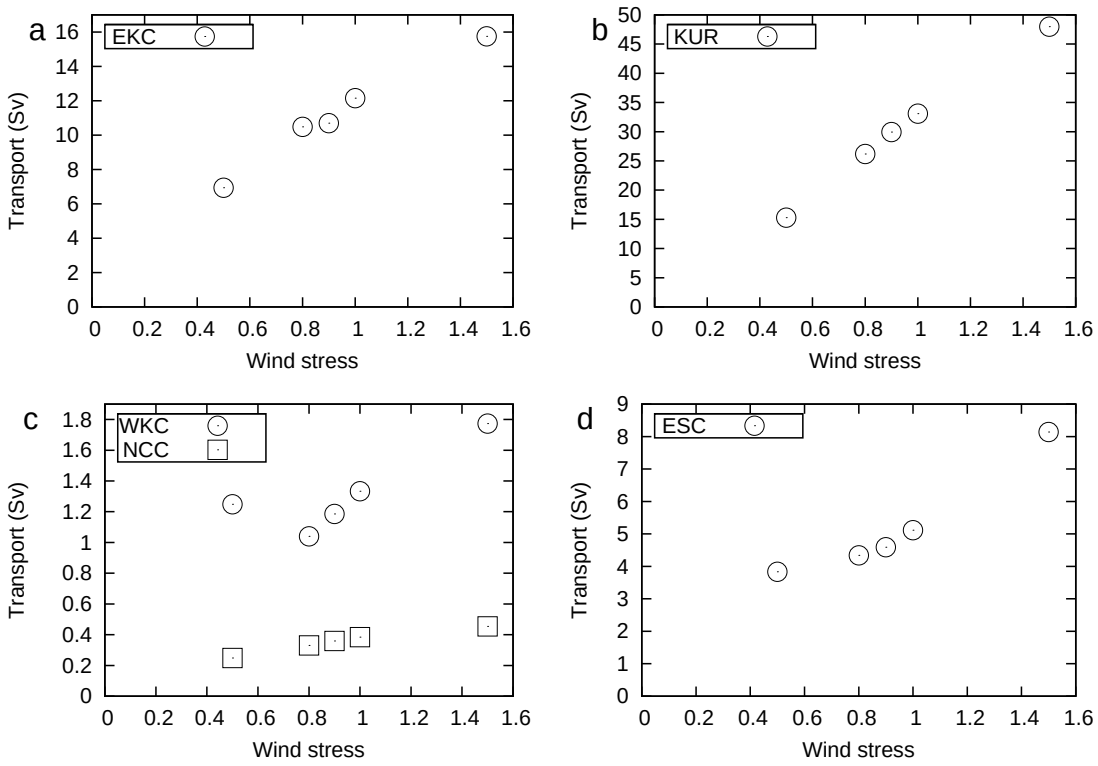

Figure 20: Transport (Sv) of currents in 2-year average vs wind stress magnitude ratio. (a) East Kamchatka Current (EKC), (b) Kuroshio (KUR), (c) West Kamchatka Current (WKC, circles) and Northern Coastal Current (NCC, squares), (d) East Sakhalin current (ESC).

(Fig. 21a), calculated by

$$\Psi(\xi, \rho) = \int^{\rho} d\rho' \frac{dz'}{d\rho'} \int h_\eta d\eta \; u_\xi(\xi, \eta, \rho')$$

where ξ and η denote the model coordinates, ρ denotes density, h_η is metric in η direction, and u_ξ is velocity in ξ direction of this model (Fig. 21e). This meridional streamfunction was made by integrating not in the east-west direction but along the curved model coordinates, because the streamfunction is sensitive to the accuracy of this integration. Further, the model coordinates are convenient since the η-component tends to follow the northwestern coast where DSW forms under the polynyas. In this definition $+\xi$ direction (nearly southward) flow and $-\xi$ direction (northward) flow on the same density cancel each other; it includes only the diapycnal transport between the surface and intermediate layers.

The overturning circulation in the Sea of Okhotsk consists of three components: West Kamchatka Current as northward transport centered at $26.8\sigma_\theta$, intermediate layer component of the East Sakhalin Current as southward transport at around 26.9–$27.0\sigma_\theta$, and the DSW formation in the continental shelf ($\xi \sim 70$–150). Over the continental shelf the axis of the lower limb (i.e., DSW) becomes lighter as it goes southward because DSW entrains surrounding lighter water. The diapycnal transport at $26.85\sigma_\theta$ in CTR has a maximum value of 1.8 Sv in March.

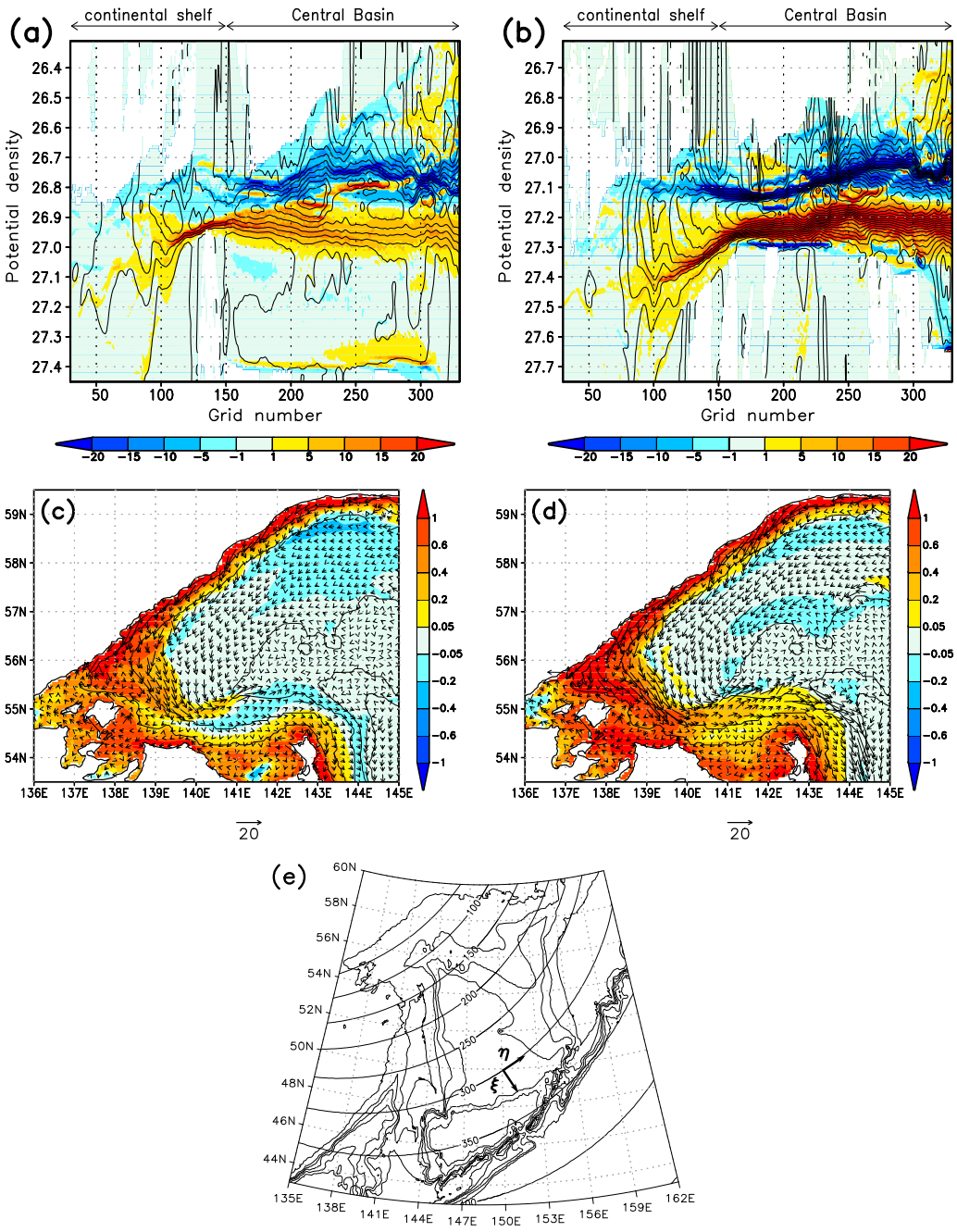

Figure 21: (a) Meridional streamfunction (Sv, contour) and transport in each isopycnal layer (Sv/1σ_θ, color) in March. The ξ-axis expresses gird numbers in the model coordinate. Contour interval = 0.2 Sv. The blue and red shades mean northward and southward flow, respectively. (b) Same as (a) but in WND1.5. (c) Horizontal velocity ($\times 10^{-2}$ m s^{-1}) and salinity anomaly (psu) at the bottom to the annual-mean of each grid in middle February in CTR. Bathymetric contours of 50, 100, 200, 500, 1000 m are drawn. (d) Same as (c) but in WND1.5. (e) Map of the model coordinate with the grid number in terms of ξ. The meridional streamfunction was made by integrating along this line. Velocity in ξ direction (u_ξ) and η direction (v_η) at a grid are also drawn.

Sensitivity of the meridional streamfunction was then examined. A 2-year mean of its maximum value of the streamfunction was defined as the meridional diapycnal transport and plotted in Fig. 22. The overturning circulation is highly sensitive to wind changes even though it represents the diapycnal transport. Figure 21b shows that the overturn is clearly intensified in the shelf region where DSW forms, compared with the overturn in Fig. 21a. This is curious because salt flux due to brine rejection is not sensitive to the wind changes as seen in previous sections.

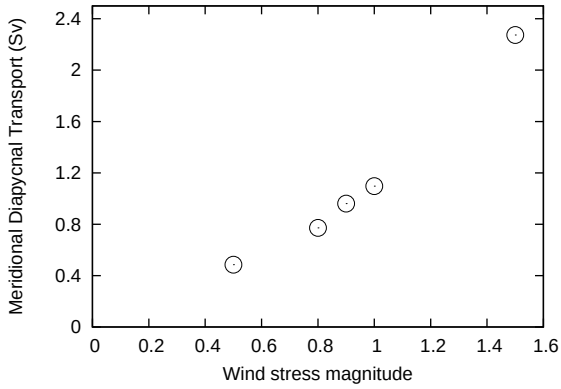

Figure 22: Transport (Sv) of the meridional overturning circulation crossing a specific isopycnal surface; maximum values of the meridional streamfunction in the Sea of Okhotsk averaged over 2 years.

To understand the sensitivity of the diapycnal transport to wind, we display Fig. 21c and Fig 21d showing horizontal velocity and salinity anomaly at the bottom to its annual mean of each grid in February. High salinity water, indicating DSW, flows along coastline as a part of the Northern Coastal Current. The water mass transformation occurs there, because the cooling and brine input provide enough buoyancy to mix the whole water column under the polynyas. Since volume flux conservation holds along the coastal current under the polynyas ($V_{\mathrm{DSW}} = V_p$, where V_{DSW} and V_p denotes volume flux of DSW and that into the polynyas, respectively; see Matsuda et al. [2009]), increased current entering the coastal polynyas results in the increased DSW outflow, implying an increase in the diapycnal transport in the shelf region by the horizontal coastal currents (compare Fig. 21a with b). In fact, in WND1.5 the increase of the transport of bottom current along the canyon off the northern coast of Sakhalin (Fig. 21d) is caused by increase of the transport of the Northern Coastal Current. In this case, DSW further entrains surrounding waters in its journey, and increase its transport remarkably during its deep ventilation; the transport in WND1.5 increases more than twice of that in CTR.

The sensitivity of the meridional streamfunction to the wind appears contradictory to the insensitivity of the DSW production defined by temperature and density criteria in the previous subsection. The increased wind results in more DSW formation in the coastal polynya, more DSW transport, and more DSW dissipation by mixing with surrounding waters in its journey. Because of mixing, the water properties tend to be modified and become out of the DSW definition, especially with respect to the potential temperature criteria by mixing surrounding warmer waters. Therefore, we consider that the diapycnal transport evaluated by the meridional streamfunction is more appropriate than that evaluated by water properties, although the latter has been conventionally done in analyses of observational data and numerical outputs.

Figure 23 is the vertical cross section along the overturning circulation; it consists of the

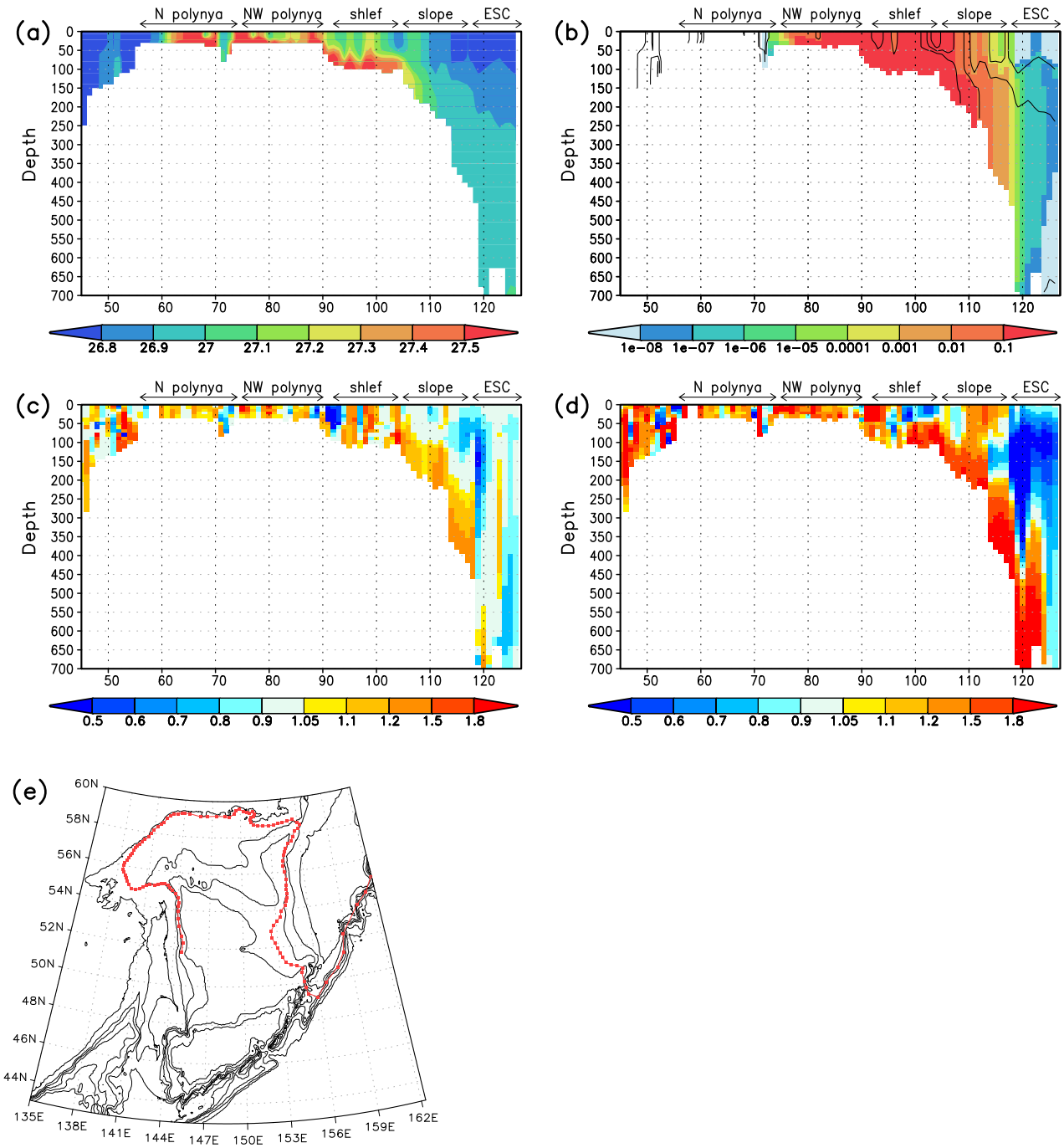

Figure 23: Cross sections along the overturning circulation of (a) potential density in late February (2/27), (b) tracer concentration on the same day in the tracer experiment (see subsection 4.4), (c) horizontal speed ratio of WND1.0 relative to CTR averaged over February, (d) same as (c) but of WND1.5 relative to WND1.0. x-axes indicate grid number along the overturning circulation, consisting of northern polynya (N polynya), northwestern polynya (NW polynya), continental shelf (shelf), continental slope (slope) and the East Sakhalin Current (ESC) as shown above each figure. (e) Map of the section line.

shallow northern and northwestern coast of 35 m depth (shallowest depth in the model), the

northwestern continental shelf of 100 m depth, and the continental slope west of the Sakhalin Island. It also includes the jet axis of the Northern Coastal Current and the East Sakhalin Current. From late November, the cooling and brine rejection causes the mixing to the shallow bottom of the coast on the Northern Coastal Current, and subsequently salinity and density grows during winter. In late December DSW begins to flow down to the continental shelf of 100 m depth. In February DSW flows down on the continental slope and intrude the intermediate layer of 200–700 m (Fig. 23a). Tracer concentration input in the northwestern continental shelf (the experiment in subsection 4.4) across the section clearly agree with this feature (Fig. 23b).

Figure 23c and d are the horizontal current speed ratio of WND1.0 to CTR and WND1.5 to WND1.0, respectively. The current speed increases especially at the coast (i.e., the Northern Coastal Current) and at bottom of continental slope (i.e., the lower component of East Sakhalin Current). This shows these currents and hence the overturning circulation depend on the wind stress through the Northern Coastal Current entering into the polynya and crossing the diapycnal surface horizontally as discussed above. These feature is summarized in Fig. 24.

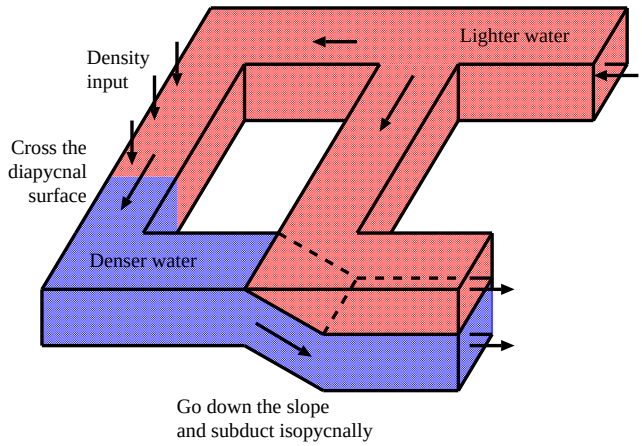

Figure 24: Schematic view of overturning circulation in the Sea of Okhotsk. The area colored red indicates the lighter water current, such as the West Kamchatka Current and westward Sverdrup current. Blue indicates the denser water current, i.e., DSW and the lower limb of the East Sakhalin Current. In the coastal polynya, cooling and brine rejection makes the water which comes into it denser. It can be seen horizontal but diapycnal transport. The denser water goes down the continental slope isopycnally and subducts under the lighter water.

5.4 Sensitivity of SSS and ventilation

The DSW salinity and density are also sensitive to wind stress as mentioned previously (Fig. 19). Only 10% increase in wind-stress strength causes more than 0.1 psu increase in SSS in the Sea of Okhotsk (from 32.29 psu in CTR to 32.44 psu in WND1.0). One of the causes of the salinity increase is enhanced salinity advection reinforced by stronger wind driven circulation, as discussed by Matsuda et al. [2009]. What is more, not only SSS in the Sea of Okhotsk but SSS in the entire subarctic gyre of the North Pacific are increased (Fig. 25). This salinity anomaly should be advected to the DSW formation region through the pathway that connects the Bering Sea and the Sea of Okhotsk as discussed in section 4. Consequently, the DSW density is changed owing to the SSS change depending on the large-scale wind stress change.

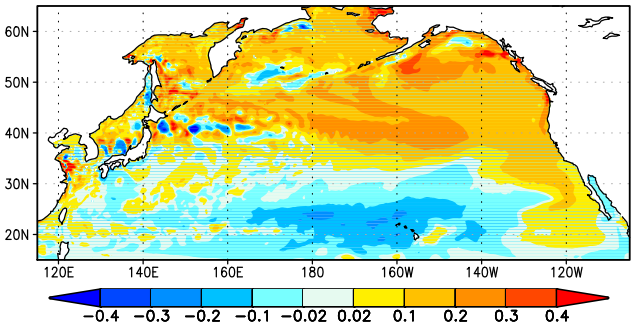

Figure 25: Annual mean SSS anomaly (psu) in WND1.0 relative to CTR. This means that a 10% increase of wind stress causes higher SSS in the subarctic region.

One of candidates that can cause the salinity anomaly in subarctic region is intergyre exchange of waters between the subarctic and subtropical gyres [d 'Orgeville and Peltier, 2009]. This exchange should vary as surface wind varies because the southward surface Ekman transport must be compensated by subsurface northward geostrophic flow transporting the subtropical water to the subarctic gyre. This is known as the subpolar cell [Lu et al., 1998; Endoh et al., 2004], and stronger wind would bring about a high-salinity anomaly to the subarctic gyre due to enhanced exchange. Another candidate of the origin of the salinity anomaly is local Ekman upwelling and winter-time mixing of the upper layer in the subarctic region. However, since salinity and thickness of the mixed layer increase with wind (Fig. 26a and b), and hence vertically integrated salt amount ($\int Sdz$, where S is salinity) increases, lateral advection of salt is necessary to compensate the salinity increase in the mixed layer. Fig. 26c shows the anomaly of vertically integrated salt amount in WND1.0 relative to CTR. The salt amount becomes larger in WND1.0 than that in CTR in almost all of the subarctic region. Considering the above, the local upwelling and/or mixing, and the lateral advection are considered to work together to cause the SSS increase in the subpolar region. Fig. 26c also exhibits relatively high salt amount anomaly in the eastern basin of the Sea of Okhotsk where the West Kamchatka Current flows, suggesting that the anomaly comes via the northern Kuril straits from the subarctic North Pacific.

In order to study the salinity advection further, a transition experiment was carried out; after the integration of CTR for 40 years, wind stress was replaced by that of WND1.0 for 20 years. The transition experiment is referred to as TRN below. Since the integration in CTR was made for 60 years, the last 20-year evolution of total salt flux was compared to the evolution in TRN.

As soon as the wind increases, the subarctic North Pacific displays higher salinity (Fig. 27a).

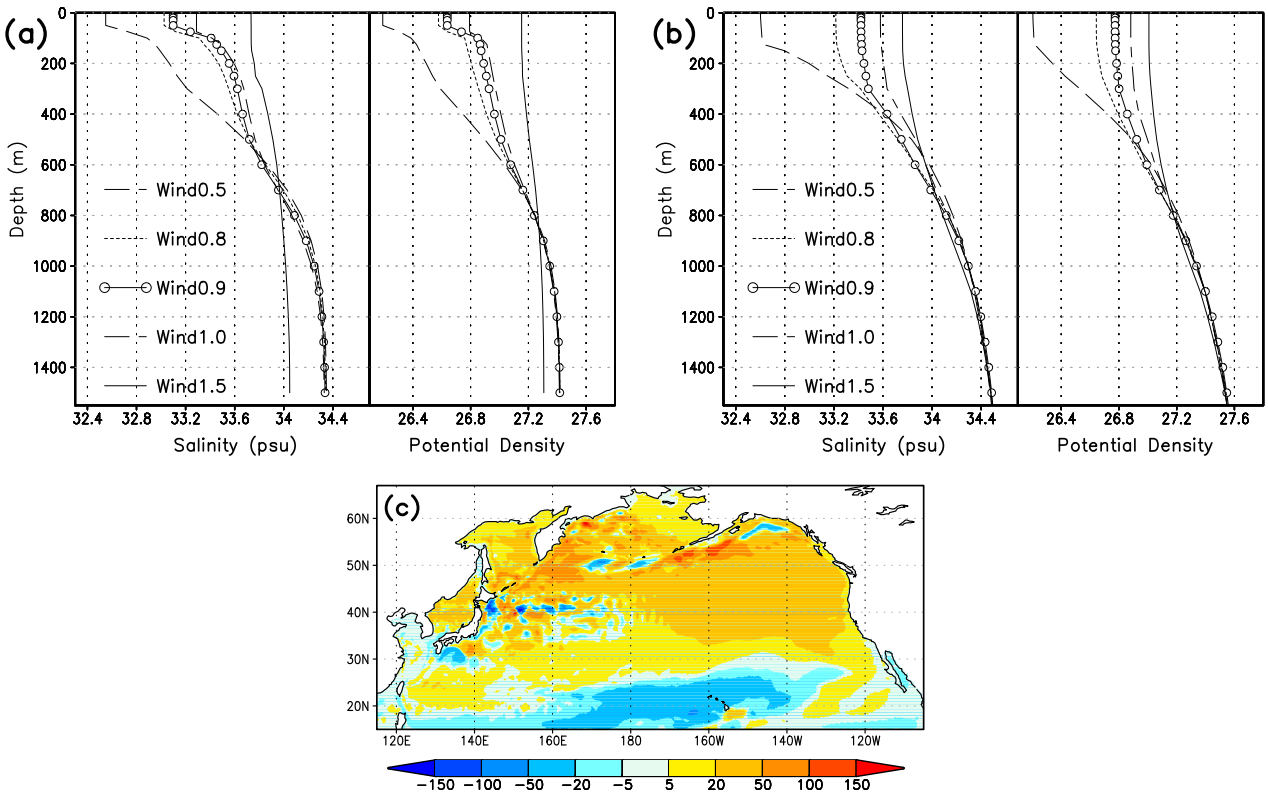

Figure 26: Vertical profiles of salinity and potential density in February at (a) 53°N, 146°E (western part of the Sea of Okhotsk), (b) 53°N, 160.5°E (in the East Kamchatka Current to the east of the Kamchatka Peninsula). (c) Anomaly of vertically integrated salinity (psu m) in WND1.0 relative to CTR.

This distribution pattern is similar to that of wind stress increase and its curl (Fig. 27b), so the local upwelling/mixing is likely responsible for SSS increase in early stage of the experiment. After integration of 5 years in TRN, however, the anomaly of the total salt amount, which gives

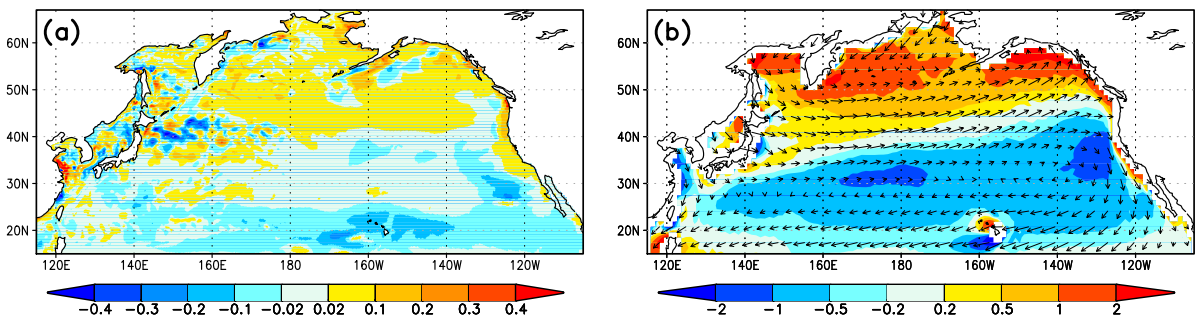

Figure 27: (a) SSS anomaly (psu) in TRN relative to CTR in December of 1st year. (b) Annual mean wind stress vector and its curl ($\times 10^{-7}$ N m^{-3}).

impacts on SSS, increases in the Kuroshio/Oyashio Extension region, as well as in the Aleutian Basin and north of 48°N in the North Pacific (Fig. 28a). To explain this transient behavior, we

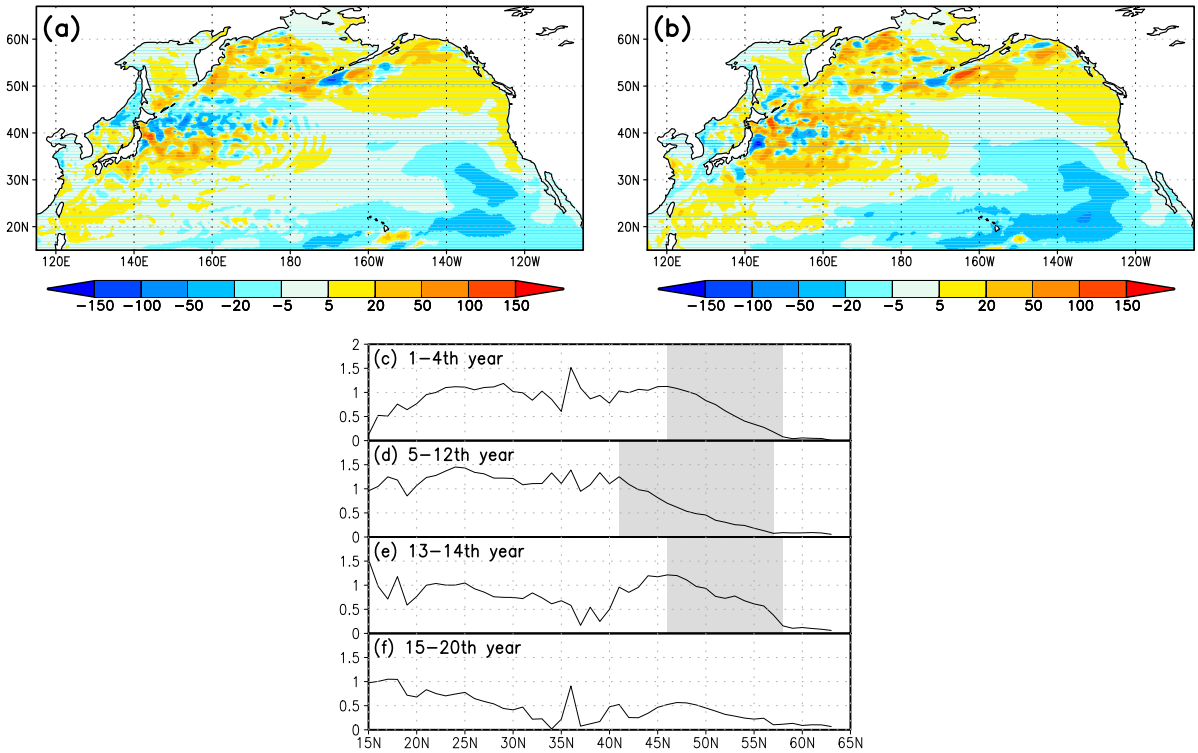

Figure 28: (a) Anomaly of vertically integrated salinity (psu m) in TRN of 4th year relative to CTR. (b) Same as (a) but 6th year. (c–f) Anomaly of northward salt flux (psu Sv) in TRN relative to CTR, averaged for (c) 1–4th year, (d) 5–12th year, (e) 13–14th year and (f) 15–20th year. The northward salt flux shows distinctive pattern in each averaging period. Shades in (c), (d) and (e) show the convergence areas of northward salt flux in the subarctic region.

consider the conservation of total salt amount in each latitude belt:

$$\frac{\partial}{\partial t}\iint dxdz\ S(x,y,z) = -\frac{\partial}{\partial y}\iint dxdz\ v(x,y,z)S(x,y,z)\ ,$$

where v is northward velocity, x, y, z are northward, eastward, upward direction, respectively. The right hand side of the equation indicates the negative gradient of northward salt flux crossing a $x-z$ section with respect to a latitude. The left hand side indicates temporal evolution of total salt amount integrated over a $x-z$ section within a latitude belt. In a steady state, since there is no gradient of northward salt flux, salt amount and hence salinity does not change. In a transition state, if the gradient of northward salt flux is positive (i.e., diverges), the salt amount there decreases. Fig. 28c–f shows the anomaly of northward salt flux in terms of latitude (anomaly of the integrand of the right hand side) in TRN relative to CTR, averaged over several years. In the period between the year 1 and 4, the northward salt flux grows in all latitude, but it converges in 46–58°N (Fig. 28c). This corresponds to the increase of salt amount in the subarctic gyre north of 48°N (Fig. 28a). In the next several years (year 5–12), the northward salt flux in the subtropics becomes largest, and it converges north of 40°N (Fig. 28d) that is the boundary between the subtropical and subarctic gyres. This corresponds to the intergyre salt transport from the subtropics via the Kuroshio/Oyashio Extension, as in Fig. 28b, associated with the increase of the Kuroshio transport. After this period, northward salt flux in the subtropics

decreases, and convergence area of it shifts northward again (Fig. 28e) for a few years. After 20 years of integration the salt flux gradually decreases (Fig. 28f) and the salt amount anomaly distribution becomes closer to a steady state similar to Fig. 26c. With these experiments and analyses, we concluded that the two mechanisms (i.e., the local upwelling/mixing and salt transport through the subpolar cell) work together to cause the increase of SSS in the subarctic gyre (Fig. 29).

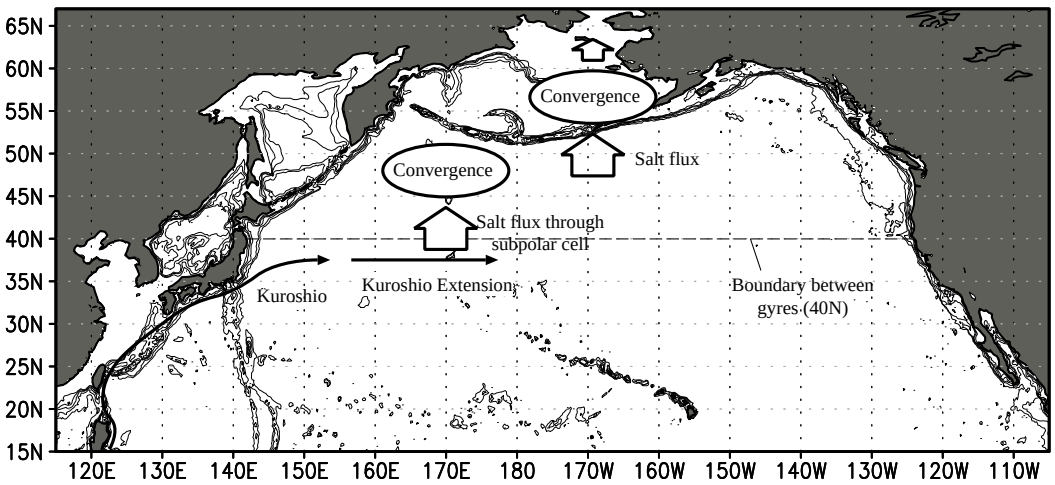

Figure 29: Schematic view of vertically integrated salt flux shown in transition experiment. In the year 1–4, the northward salt flux converges in 46–58°N and salt amount increase there. In the year 5–12, the intergyre transport advects the salt from the subtropic gyre to the subarctic gyre.

The wind variations cause significant changes not only in SSS, but also in density stratification in the Sea of Okhotsk (Fig. 26a). Since the salinity (and hence density) stratification in the East Kamchatka Current also decreases as wind strengthens (Fig. 26b), the deep mixed-layer water originating in the Bering Sea is responsible for the decrease in stratification in the Sea of Okhotsk.

These stratification changes cause variations in the subsequent ventilation. Contrary to CTR, the WND0.5 case indicates that the currents is surface intensified and confined to upper 400m (Fig. 30a). Ventilation of cold water to the intermediate layer does not occur in this case, consistent with the shutdown of DSW production discussed in the previous section. On the other hand, the current extends from surface to bottom in WND1.5 (Fig. 30b), where stratification in the Sea of Okhotsk almost totally breaks down.

In order to see the deep ventilation in WND1.5, we display Fig. 30c to show a cross section of the potential temperature in the central basin in February. Due to the DSW intrusion extending to the bottom, cold water occurs throughout the water column in the western part of the Sea of Okhotsk. On the other hand, the eastern part keeps a warm temperature caused by the inflow of the North Pacific water from the East Kamchatka Current. DSW ventilates bottom waters deeper than 1000 m in the Sea of Okhotsk, since DSW becomes heavier than the North Pacific water owing to the brine input under the polynyas. In conjunction with the increase

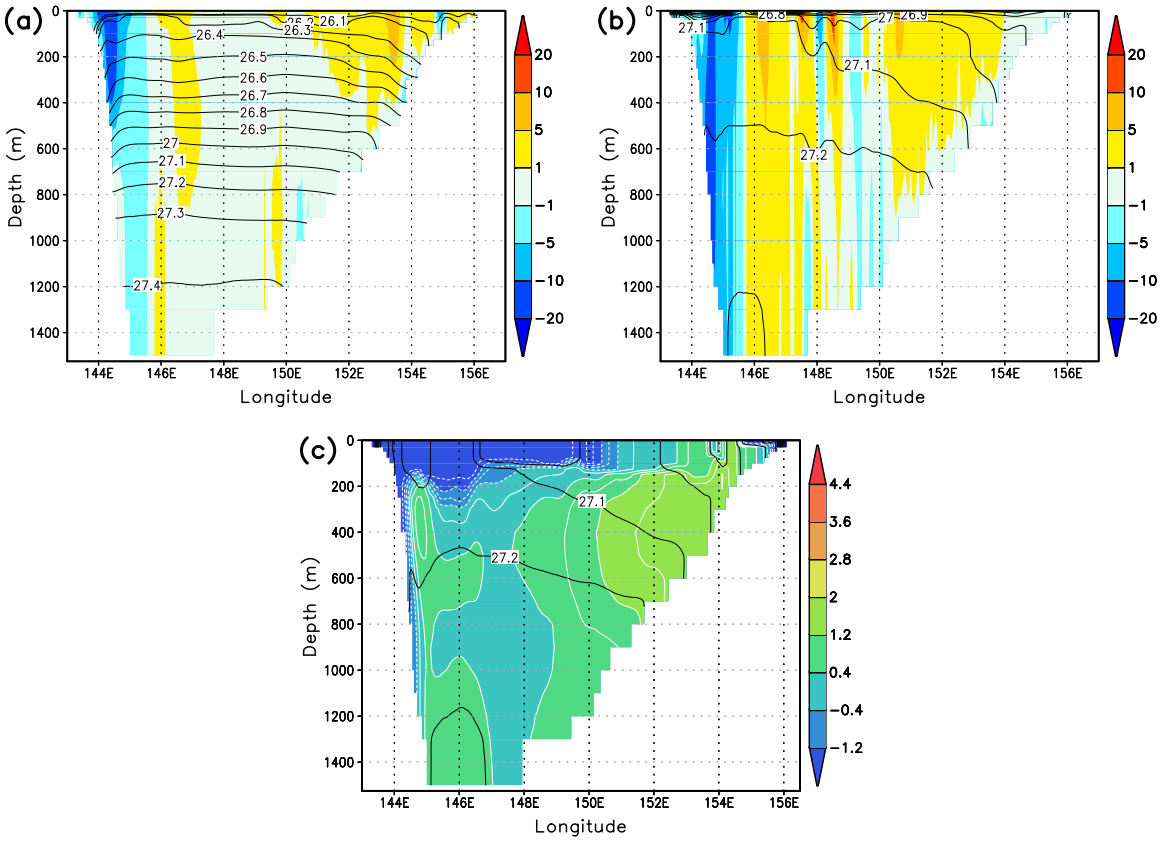

Figure 30: Cross sections across 53°N of northward velocity ($\times 10^{-2}$ m s^{-1}, color) and potential density (contour) in May in (a) WND0.5 and (b) WND1.5. (c) Same as (b) but potential temperature (color) and potential density (contour) in February.

of the overturning transport as in Figs. 21b and 22, we conclude that the ventilation and the overturning circulation are strengthened by intensified wind.

6 Sensitivity of SSS in the Sea of Okhotsk and overturn to fresh water flux

We next examined the sensitivity to fresh water flux from the Bering Sea. As shown in the tracer experiment from the Bering Sea, Bering Sea water is advected to the Sea of Okhotsk by the coastal current, inshore branch of the East Kamchatka Current. The variations of the eastern Bering Sea can be well conveyed to the Sea of Okhotsk and affect SSS in the Sea of Okhotsk and then overturning circulation.

Climate change of recent global warming will result in not only warmer air temperature but also stronger wind and more precipitation and river runoff. On the other hand, in the Last Glacial Maximum, there were less river runoff in subarctic region, and lowered sea level followed by closing of the Bering Strait. If the Bering Strait closes, through which the fresher water goes northward to the Arctic Ocean, the fresher water can be advected to the west of Bering Sea, the Sea of Okhotsk and to the intermediate layer of the Sea of Okhotsk and North Pacific

by the overturning circulation. It can change SSS in the Sea of Okhotsk, DSW density, and stratification in the Sea of Okhotsk. Similarly, a change of river runoff can affect them, too. Matsuda et al. [2009] showed the Amur river discharge may shutdown the subduction at the east coast of Sakhalin Island by strengthening of stratification.

So we show the sensitivity experiments of (1) No Bering Strait throughflow (referred as NBT), (2) No river runoff in the Sea of Okhotsk upstream of mouse of the Amur River and in the Bering Sea adjacent to the Eurasia Continent (referred as NR), (3) 1 and 2, that is, no Bering Strait throughflow and no river runoff (referred as NRBT). The last 2 years of 40 years integration were used for analysis.

Figure 31 shows the SSS anomaly of each experiment relative to CTR. In NBT a low salinity anomaly flows along the northern coast of the eastern Bering Sea, and enter into the Sea of Okhotsk. This is consistent to the tracer experiment in subsection 4.2. The low salinity anomaly spreads in the Sea of Okhotsk and the North Pacific widely. Moreover, it is notable that it is fresher in the Sea of Okhotsk than in the Bering Sea.

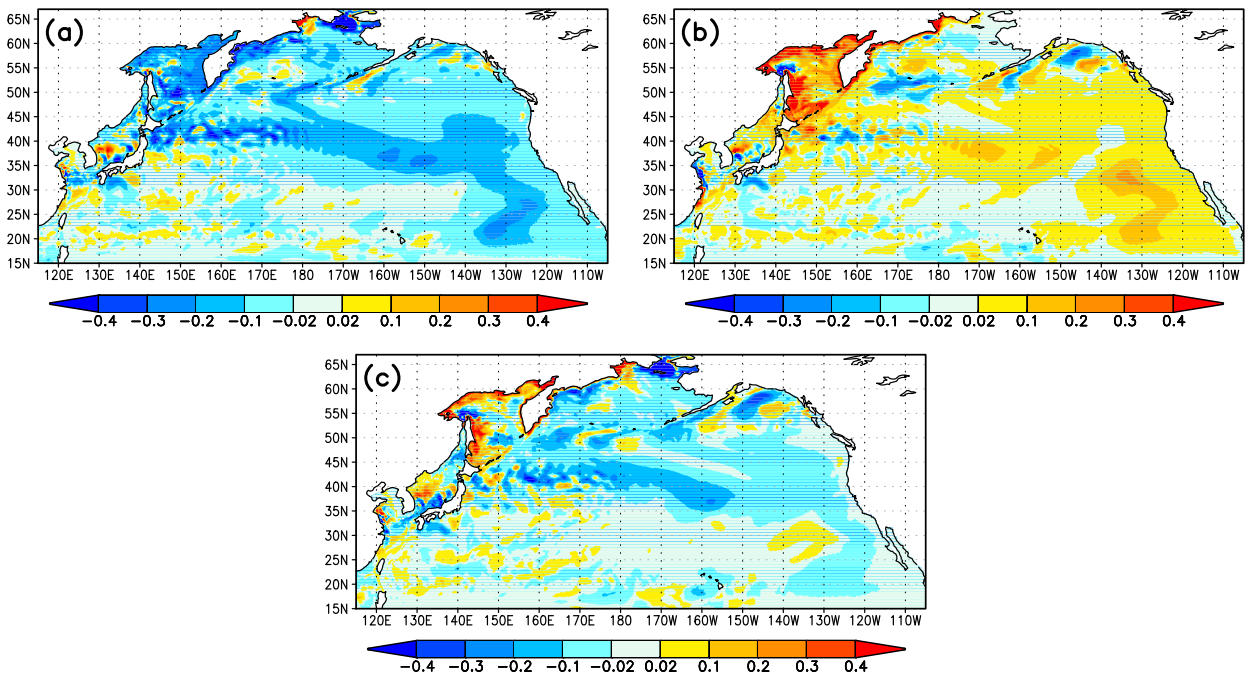

Figure 31: Annual mean SSS anomaly (psu) in (a) NBT, (b) NR, (c) NRBT relative to CTR.

In NR high salinity anomaly can be seen along the coastline because of the lack of river runoff. The impact of river runoff is restricted to near the coastline in the Bering Sea, but in the Sea of Okhotsk it intrudes the interior.

SSS anomalies in the Sea of Okhotsk are −0.17, +0.42 and +0.26 psu in NBT, NR and NRBT, respectively. In NBT it is fresher than that in WND0.8, and in NR it is saltier than that in WND1.0; in the both experiments the effect of fresh water is great. In NRBT, it is almost linear combination of the NBT and NR. The effect of river runoff is greater than that of Bering Strait throughflow for SSS in the Sea of Okhotsk, while less in the Bering Sea and the North Pacific.

The meridional transports calculated by overturning circulation are 0.95, 1.47, 1.27 Sv in NBT, NR and NRBT, respectively. Since it is 0.96 Sv in CTR, the meridional transport is

not sensitive to the Bering Strait throughflow and SSS in the Sea of Okhotsk at least directly. However in NR, it is larger than CTR by ∼50%. Further the increase of the meridional transport is relaxed by the fresher water from the Bering Sea in NRBT. These results suggest that fresh water input into the polynyas makes the strong halocline that prevents the penetration of brine rejection and overturning circulation. NRBT shows that in the glacial epoch SSS in the Sea of Okhotsk was saltier, and the overturning circulation was stronger than today if only the effect of freshwater is considered.

7 Conclusion and Discussion

We succeeded in representing the three-dimensional structures of the intermediate overturning circulation in the North Pacific. In particular, we described a detailed surface pathway from the Bering Sea to the northwestern shelf of the Sea of Okhotsk where dense shelf water (DSW) forms owing to brine rejection, as well as the intermediate-layer pathway caused by the subsequent ventilation. These pathways are linked by narrow boundary currents, coastal currents and flows through straits as summarized in the subsection 4.5 and Fig. 15.

We further examined sensitivity of the overturning circulation to wind stress using this model which represents the three-dimensional structure properly. The results of numerical experiments are as follows:

- Sensitivity experiments revealed that the overturning circulation, evaluated by the meridional streamfunction, is sensitive to wind stress, although ice production (i.e., brine rejection) is not very sensitive. This indicates that the volume transport by the wind-driven coastal current is an important parameter for quantifying the diapycnal transport associated with the overturning circulation. Since mixing due to brine rejection is intensive enough to mix the whole water column under the polynyas, all surface water entering coastal polynyas by wind-driven currents is likely transformed into DSW. This causes increase in the volume flux of the diapycnal transport in the polynyas and the subsequent ventilation when the wind stress increases.

- SSS in the Sea of Okhotsk and the subarctic North Pacific also depends on wind stress significantly. Advection of saline water from the subtropical ocean is responsible for this subarctic SSS sensitivity to wind.

- The SSS changes cause marked changes in salinity stratification. As the wind is strengthened, the increased SSS in the Bering Sea and the Sea of Okhotsk causes growth of the mixed layer thickness. In the Sea of Okhotsk, further, the SSS changes are conveyed to the intermediate layer accompanied by the DSW subduction. As a result, the increase of the diapycnal transport and the weakening of stratification act together to allow intense overturn and deep ventilation. DSW may subduct even to the bottom of the Sea of Okhotsk if the wind is extremely strong.

We also examined the sensitivity to fresh water flux and found that salinity variations in the eastern Bering Sea well propagates to the Sea of Okhotsk, and affects SSS in the Sea of Okhotsk and then overturning circulation. It also suggested the picture of the overturning circulation in the glacial epoch.

The meridional diapycnal transport of the overturning circulation was found to be attributed to the Northern Coastal Current. The transport of The Northern Coastal Current is 0.36 Sv in

average, but it has seasonal variation, with the maximum 0.85 Sv in November (Fig. 32a). Here we discuss the mechanism to drive the Northern Coastal Current. The first candidate of the mechanism is the sea surface Ekman transport by local wind stress just above the measurement line, calculated by

$$Q = \int dy \, \frac{\tau_y}{\rho f} \ .$$

The Ekman transport calculated by above integration from 58.00°N to 59.35°N along 147.375°E (in which the OMIP data are arranged) is 0.03 Sv in average over a year (Fig. 32b). It records maximum of 0.11 Sv in December.

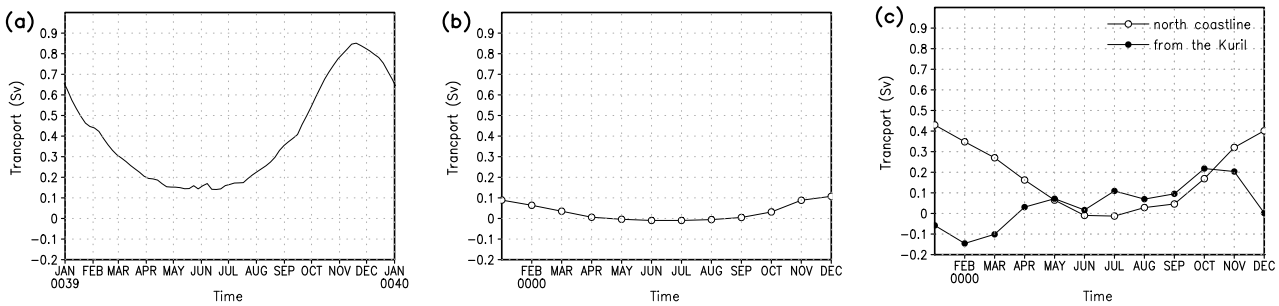

Figure 32: (a) Seasonal variability of transport (Sv) of the Northern Coastal Current. (b) Estimated transport (Sv) by surface Ekman transport mechanism. (c) Same as (b) but by ATW.

Second candidate is arrested topographic wave (ATW; [Csanady, 1978]) formulated as:

$$Q = \int \boldsymbol{\tau} \cdot d\boldsymbol{l}/\rho f \ ,$$

where $\boldsymbol{\tau}$ is wind stress vector and $d\boldsymbol{l}$ is the line element along the integration. This is the integration of wind stress from a long distance, not local one. The transport calculated by the formula with wind stress data from OMIP is 0.19 Sv in average, with the maximum of 0.43 Sv in January (Fig. 32c) if it is integrated along the north coastline (58.878°N from 155.25°E to 147.375°E). If integrated from the Kuril island (from 51.028°N to 155.25°E), it reduced to be 0.04 Sv with the maximum of 0.22 Sv in October because the wind stress west of the Kamchatka Peninsula makes the circulation of opposite direction by this mechanism. Although the route of integration was rough and the resolution of the wind stress data was inadequate ($\sim 1.125°$), the estimated transport is smaller than the total transport (0.36 Sv).

In order to study these two mechanisms further, we conducted a wind-cease experiment; after 41 years integration of CTR, wind stress was replaced by null all over the domain. The averaged transport in 3rd and 4th year of the Northern Coastal Current is 0.25 Sv: less than that in CTR by 0.11 Sv, which is attributed to the summation of the surface Ekman transport and ATW. This value is between the value if integrated from the Kuril islands as ATW, 0.08 Sv, and the value if integrated only along the north coastline, 0.22 Sv. After the wind ceased, the seasonality retains although there is no seasonality by wind stress (Fig. 33a). There are only seasonalities by heat flux, fresh water flux and restoring effect far from the Sea of Okhotsk. Something may propagate remotely to the Sea of Okhotsk. However, the transports of the Kuroshio and the East Sakhalin Current fall down in about 3 years and 2 months, respectively (Fig. 33b, c).

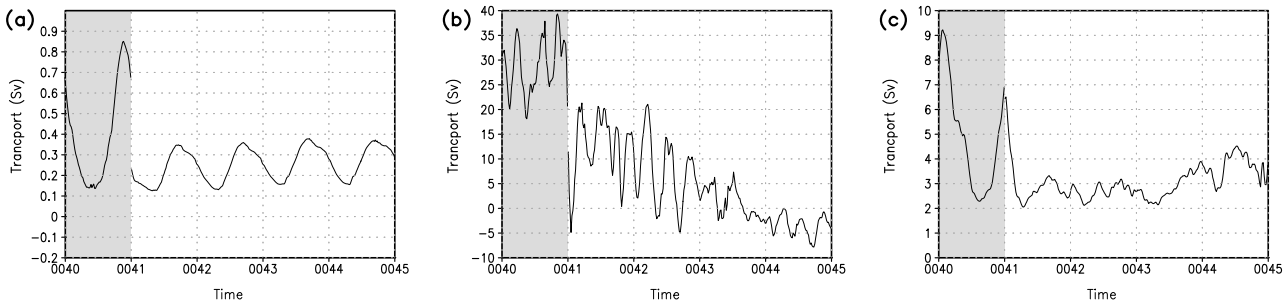

Figure 33: (a) Variation of transport (Sv) of the Northern Coastal Current in the wind ceased experiment. Shade denotes that of CTR. (b) Same as (a) but the Kuroshio's (c) Same as (a) but the East Sakhalin Current.

Third candidate is density current trapped to the coastline by the river fresh water input. The river runoff upstream of 147°E in the Sea of Okhotsk is 0.01 Sv, but it may entrain the surrounding sea water and form the density current with geostrophic balance. In order to study this possibility, we conducted a no-river experiment; after 41 years of integration of CTR, all fresh water input by river were cut-off. Precipitation and evaporation retained the same as CTR. The averaged transport in 3rd and 4th year of the Northern Coastal Current is 0.29Sv: less than that in CTR by 0.07 Sv, which is attributed to the river runoff.

The rest of 0.36 Sv is 0.18 Sv which remains to be explain. Figure 34a shows cross sections of potential density and westward velocity in October at 147°E in CTR. There is a density stratification derived from both salinity and temperature stratification in the interior. On the other hand, near the coastline the density stratification deepens as it goes northward, and the contours of density lean to the north. Just at the position of leaning, there is the core of the Northern Coastal Current with the geostrophic balance. A reason why the contours of density lean is northward flow. A northward flow at sea surface is compensated by bottom Ekman flow, which goes down the slope entraining the shallower water. As a result, contours of density leans and it makes the westward current with the geostrophic balance.

However, even in the case of no wind (Fig. 34b), the contours of density lean and the Northern Coastal Current revives in summer though it is weaker than that in CTR. This is because that the stratification is weaker in the coastal area than in the offshore and it is easier to penetrate it by vertical mixing such as tidal mixing. Since the surface lighter water reaches the bottom in the coastal area in winter and it remains at bottom in summer, the stratification becomes weaker and it is easier to penetrate in turn in autumn. Then, the horizontal gradient of potential density and the Northern Coastal Current revive in every autumn.

As for another candidate, we note that the inflow through the Onekotan Strait and the 1st Kuril Strait is 0.23 Sv in total: same order as the transport of Northern Coastal Current. Okhotsk-North Pacific water exchange might have relation with the Northern Coastal Current with the mechanism such as coastal wave or sea level difference, etc. In addition, the Sverdrup balance with topography should be studied.

One of our challenges in this study was to simulate the North-Pacific-scale SSS without restoring to observed SSS. This previously has been scarcely done in modeling of the mid- and high-latitude ocean areas. As seen in the previous sections, our model tends to exhibit high SSS in the subarctic gyre, although overall SSS features are comparable to the observations. We have

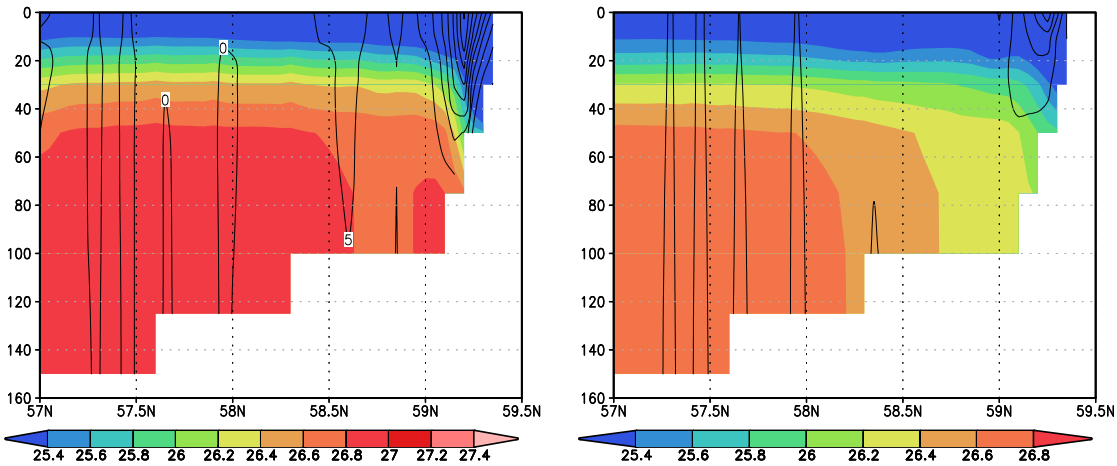

Figure 34: Cross sections at 147°E of density (color) and westward velocity (contour, contour interval = 0.05 m s^{-1}) in October. (a) CTR in 40th year. (b) no wind case in 44 th year.

not yet identified the cause of the high SSS bias, even though we indeed examined the sensitivity to various effects such as precipitation minus evaporation ($P - E$) and tidal mixing, in addition to changing the wind strength as discussed. In the present study, based on the SSS sensitivity in the subarctic gyre to wind, we adopted the case with the wind stress multiplied by a factor of 0.9 as the control case, rather than the WND1.0 case, to describe model characteristics as shown in Section 3 and 4. Nevertheless, wind-driven circulations and associated transports (e.g. the Kuroshio's) appear to be better represented quantitatively in the WND1.0 case. Since the saline water is supplied only from the lower latitude through the oceanic pathways, it is important to investigate further the intergyre exchange between the subarctic gyre and the subtropical gyre in order to better understand the controlling factors for SSS, in addition to better estimation of $P - E$.

The impacts of the SSS changes on the simulated stratification and the ventilation in the Sea of Okhotsk were significant. In reality, a SSS freshening of ∼0.1 psu has occurred in the Sea of Okhotsk and the subarctic gyre in the last 50 years [Durack and Wijffels, 2010; Uehara et al., 2014]. The freshening may be a reflection of enhanced hydrological cycle caused by recent global warming [Durack and Wijffels, 2012]. Corresponding to the surface freshening, DSW intrusion into the intermediate layer and associated material transport appears to have been shifted to lighter layers [Watanabe et al., 2013]. Our model represents the DSW intrusion consistent with the above observations, although SSS anomalies in this study are not caused by precipitation changes but by wind stress variations. There were also decadal scale variations in SSS with the amplitude of ∼0.2 psu in the subarctic gyre [Uehara et al., 2014]. Our study suggests the importance of the intergyre salt flux and its variations for the decadal SSS variations, because it takes about two decades for the transient response of the subarctic SSS to settle down (Fig. 28).

Another challenge we made was to incorporate a tide generating force explicitly in simulating the large-scale overturning circulation. Previous observational and modeling studies found that tide induces profound impacts on the salt pathways and the overturn. Tidal mixing around the Kuril Straits [e.g. Nakamura and Awaji, 2004; Osafune and Yasuda, 2012] and the Aleutian Passes [e.g. Nakamura et al., 2010; Osafune and Yasuda, 2013] is particularly important as it

entrains relatively high salinity water from the deep layer to the surface; tidal mixing produces saline-water sources along the overturning pathways. Further, tide also regulates water exchange between the Sea of Okhotsk and the North Pacific through residual circulations around the Kuril Islands [e.g. Nakamura et al., 2000; Nakamura et al., 2012]. As for the large scale modeling, tidal mixing is usually parameterized as enhanced vertical diffusivity along the straits [e.g. Nakamura et al., 2006; Uchimoto et al., 2011; Osafune and Yasuda, 2012]. However, the residual circulation cannot be generated by this parameterization. In our model, instead, tide was forced explicitly, where enhanced vertical diffusion was calculated by the turbulent closure scheme of Noh and Kim [1999] (see Fig. 8), whereas the residual circulation is generated directly although the resolution may not be sufficient [e.g. Nakamura et al., 2012].

Effects of the direct tidal forcing were notable. For example, the net inflow transport across the northern Kuril Straits including the Kruzenshtern Strait and the Onekotan Strait (see Fig. 1) was 3.9 Sv in the present control case. However, it reduced to about 0.3 Sv if the direct tidal forcing was ceased (but for the enhanced vertical diffusion being applied). Therefore, the direct tidal forcing is likely important to simulate the salt water exchange between the North Pacific and the Sea of Okhotsk. We do not pursue this further here because the tidal effects need more focused studies. Higher resolution may be necessary to evaluate more quantitatively the exchange through the Kuril Straits caused by residual circulations and intensive submesoscale eddies [Nakamura et al., 2012].

Only K1 partial tide was given in this model, but other partial tides were not, although K1 partial tide has most impact on the Sea of Okhotsk. However, in order to represent SSS and the overturning circulation precisely, the other partial tides are needed. The reason the other partial tide was not given is because the tidal flow is enough strong to diverge numerically at the narrow and steep straits of the Kuril straits such as Rasshua Strait, where the amplitude of oscillatory transport exceeds 2.2 Sv.

Appendix

A Preliminary experiment of tidal forcing

The results of the preliminary experiment of the tidal forcing are described here. K1 partial tide was used in the model, without any other forcing such as wind stress or surface heat flux. Numerical integration was done for a month with initial conditions of no stratification and no flow. The last 1 day was used for analysis here.

Fig. A1 shows speed at sea surface averaged over 1 cycle of the K1 partial tide. The results were compared to that by a global model of ocean tides which best-fits the Laplace Tidal Equations and along track averaged data from TOPEX/Poseidon and Jason (TPXO, Egbert and Erofeeva [2002]). Distribution of it was similar to each other; it has a large velocity in the northwest of the Sea of Okhotsk, west of the Bering Sea, and around the Kuril Islands and Aleutian Islands.

It is expected tidal forcing produce the residual flow [e.g., Nakamura et al., 2000]. In order to evaluate it, a tracer was input into the surface layer of the Bussol Strait in the tidal model. The tracer spreads near the straits, but it starts to go around the Bussol Island on the right hand side (Fig. A2) although it is slower than that in the high resolution tidal model [Nakamura et al., 2000].

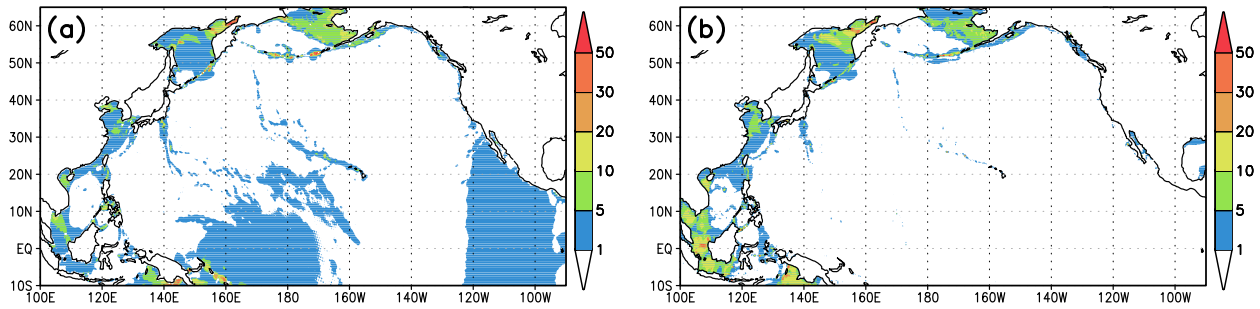

Figure A1: (a) Speed at sea surface ($\times 10^{-2}$ m s^{-1}) averaged over 1 cycle of the K1 partial tide in the case of tidal forcing only; no stratification and no atmospheric boundary condition were applied. (b) Same as (a) but by TPXO.

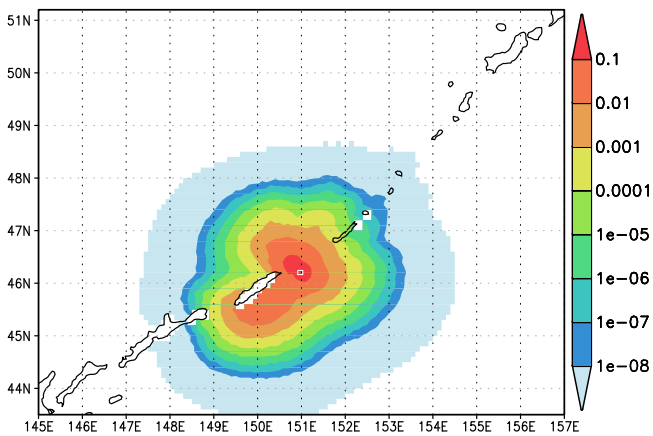

Figure A2: Tracer concentration at the sea surface, 150 days after it was input. White rectangular denotes where the tracer was input.

B Note for conversion of wind stress data

When we covert and interpolate the wind stress data from longitude-latitude coordinate to the model coordinate, we must be careful about the treatment of the data on land. In this dissertation we use the wind stress data converted simply, not cared. We consider the case northward uniform wind stress in the ocean adjacent to the land where wind stress is stronger (Fig. A3). There should be downwelling properly near the coastline because the Ekman transport goes on shore which is compensated by downwelling. However, if the data was converted simply, the data on land contaminates those on ocean in interpolation, resulting in the upwelling because of positive $(\boldsymbol{\nabla} \times \boldsymbol{\tau})_z$ (Fig. A3a). To avoid this, we replaced the data on land by 0 and interpolated in this appendix, which results in downwelling by negative $(\boldsymbol{\nabla} \times \boldsymbol{\tau})_z$ and is consistent the proper ocean dynamics (Fig. A3b).

With this properly converted wind stress data we integrated for 40 years. Figure A4 shows the SSS anomaly to WND1.0. Along the coastline it is fresher than WND1.0 as expected, but the total effect is not great.

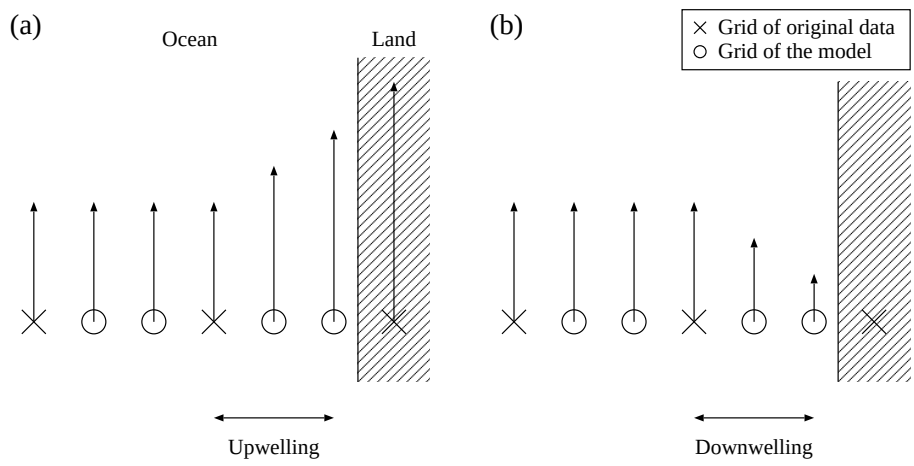

Figure A3: Illustration about wind stress data conversion and interpolation.

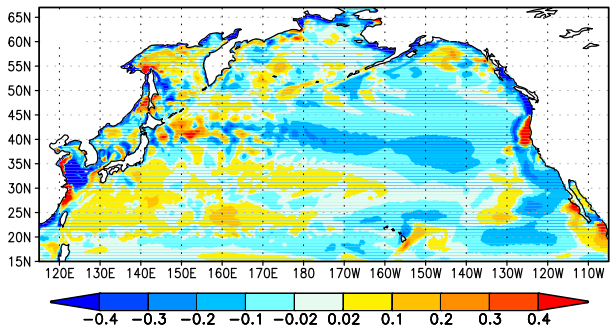

Figure A4: Annual mean SSS anomaly (psu) to WND1.0 in the case of proper wind stress.

Acknowledgments

I specially thank to Prof. H. Mitsudera for his support and patience. I'm grateful to Dr. H. Hasumi and Dr. Y. Sasajima to allow me to use the excellently arranged OGCM. I'm also grateful for their advices and discussions to Dr. M. Nonaka, Prof. K. I. Ohshima, Dr. T. Nakamura, Prof. M. Wakatsuchi, Prof. A. Kubokawa, Prof. Y. Tanimoto, Dr. J. Nishioka, Dr. Y. Fukamachi, Dr. G. Mizuta, Dr. H. Uehara, Dr. K. Uchimoto, Dr. T. Nakanowatari, Dr. Y. Matsumura, Dr. K. Kusahara, Dr. K. Ono, Dr. H. Abe, and my colleagues and friends in Hokkaido University and the Oceanographic Society of Japan.

This work was supported by Grants-in-Aid for Scientific Research No. 22221001 and No. 22106010. I was supported by JSPS Research Fellowships for Young Scientists and Global COE Program "Establishment of Center for Integrated Field Environmental Science", Hokkaido University. Data analyses were conducted with the Pan-Okhotsk Information System. Figures were drawn with GrADS, gnuplot and Tgif.

References

[*Bryden and Imawaki*(2001)] Bryden, H., and S. Imawaki (2001), Ocean heat transport, in Ocean circulation and climate: observing and modelling the global ocean, *International Geophysics Series*, vol. 77, edited by G. Siedler, J. Church, and J. Gould, pp. 455–474, Academic Press.

[*Chapman and Gawarkiewicz*(1997)] Chapman, D., and G. Gawarkiewicz (1997), Shallow convection and buoyancy equilibration in an idealized coastal polynya, *J. Phys. Oceanogr.*, *29*, 555—566.

[*Csanady*(1978)] Csanady, G. T. (1978), The Arrested Topographic Wave. *J. Phys. Oceanogr.*, *8*, 47-62.

[*Dai and Trenberth*(2002)] Dai, A., and K. E. Trenberth (2002), Estimates of freshwater discharge from continents: Latitudinal and seasonal variations, *J. Hydrometeorol.*, *3*, 660–687.

[*Durack and Wijffels*(2010)] Durack, P. J., and S. E. Wijffels (2010), Fifty-year trends in global ocean salinities and their relationship to broad-scale warming, *J. Climate*, *23*, 4342—4362, doi:http://dx.doi.org/10.1175/2010JCLI3377.1.

[*Durack et al.*(2012)] Durack, P. J., S. E. Wijffels, and R. J. Matear (2012), Ocean salinities reveal strong global water cycle intensification during 1950 to 2000, *Science*, *336*(6080), 455–458, doi:10.1126/science.1212222.

[*d 'Orgeville and Peltier*(2009)] d 'Orgeville, M., and W. R. Peltier (2009), Implications of both statistical equilibrium and global warming simulations with CCSM3. part I: On the decadal variability in the North Pacific Basin, *J. Climate*, *22*, 5277—5297, doi: http://dx.doi.org/10.1175/2009JCLI2428.1.

[*Egbert and Erofeeva*(2002)] Egbert, G., and S. Erofeeva (2002), Efficient inverse modeling of barotropic ocean tides, *Journal of Oceanic and Atmospheric Technology*, *vol. 19, N2.*

[*Endoh et al.*(2004)] Endoh, T., H. Mitsudera, S.-P. Xie, and B. Qiu (2004), Thermohaline structure in the subarctic North Pacific simulated in a general circulation model, *J. Phys. Oceanogr.*, *34*, 360—371.

[*Foreman et al.*(2006)] Foreman, M. G. G., P. F. Cummins, J. Y. Cherniawsky, and P. Stabeno (2006), Tidal energy in the Bering Sea, *Journal of Marine Research*, *64*(6), 797–818(22).

[*Fukamachi et al.*(2004)] Fukamachi, Y. and G. Mizuta and K. I. Ohshima and L. D. Talley and S. C. Riser and M. Wakatsuchi (2004), Transport and modification processes of dense shelf water revealed by long-term moorings off Sakhalin in the Sea of Okhotsk. *Journal of Geophys. Res.*, *109* doi:10.1029/2003JC001906

[*Gladyshev et al.*(2000)] Gladyshev, S., S. Martin, S. Riser, and A. Figurkin (2000), Dense water production on the northern Okhotsk shelves: Comparison of ship-based spring-summer observations for 1996 and 1997 with satellite observations, *Journal of Geophysical Research*, *105(C11)*, 26,281—26,299, doi:10.1029/1999JC000067.

[*Hasumi*(2006)] Hasumi, H. (2006), CCSR Ocean Component Model (COCO) Version 4.0, *AORI Report*, *No. 25*.

[*Imawaki et al.*(2001)] Imawaki, S., H. Uchida, H. Ichikawa, M. Fukasawa, and S. Umatani (2001), Satellite altimeter monitoring the Kuroshio Transport south of Japan, *Geophysical Research Letters*, doi:10.1029/2000GL011796.

[*Itoh*(2007)] Itoh, M. (2007), Warming of intermediate water in the Sea of Okhotsk since the 1950s, *J. Oceanogr.*, *63*, 637—642.

[*Itoh et al.*(2003)] Itoh, M., K. Ohshima, and M. Wakatsuchi (2003), Distribution and formation of Okhotsk Sea Intermediate Water: an analysis of isopycnal climatological data, *J. Geophys. Res.*, *108*, C83,258, doi:10.1029/2002jc001950.

[*Katsumata and Yasuda*(2010)] Katsumata, K. and I. Yasuda (2010), Estimates of non-tidal exchange transport between the Sea of Okhotsk and the North Pacific. *J. Oceanogr.*, *66*(4), 489–504.

[*Kawaguchi and Mitsudera*(2009)] Kawaguchi, Y., and H. Mitsudera (2009), Effects of alongshore wind on dsw formation beneath coastal polynyas: application to the Sea of Okhotsk., *J. Geophys. Res.*, *114*, C10013.

[*Kitani*(1973)] Kitani, K. (1973), An oceanographic study of the Okhotsk Sea: Particularly in regard to cold waters, *Bull. Far Seas Fish. Res.*, *Lab 9*, 45–77.

[*Kurashina et al.*(1967)] Kurashina, S., K. Nishida, and S. Nakabayashi (1967), On the open water in the southeastern part of the frozen Okhotsk Sea and the current through the Kuril Island, *J. Oceanogr. Soc. Japan.*, *23*, 57–62, in Japanese.

[*Lu et al.*(1998)] Lu, P., J. P. McCreary, and B. A. Klinger (1998), Meridional circulation cells and the source waters of the Pacific equatorial undercurrent, *J. Phys. Oceanogr.*, *28*, 62—84.

[*Matsuda et al.*(2009)] Matsuda, J., H. Mitsudera, T. Nakamura, K. Uchimoto, T. Nakanowatari, and N. Ebuchi (2009), Wind and buoyancy driven intermediate-layer overturning in the Sea of Okhotsk, *Deep Sea Research Part I: Oceanographic Research Papers*, *56*(9), 1401 – 1418, doi:http://dx.doi.org/10.1016/j.dsr.2009.04.014.

[*Mizuta et al.*(2003)] Mizuta, G., Y. Fukamachi, K. Ohshima, and M. Wakatsuchi (2003), Structure and seasonal variability of the East Sakhalin Current, *J. Phys. Oceanogr.*, *33*, 2430—2445.

[*Nakamura and Awaji*(2004)] Nakamura, T., and T. Awaji (2004), Tidally induced diapycnal mixing in the Kuril Straits and its role in water transformation and transport: A three-dimensional nonhydrostatic model experiment, *J. Geophys. Res.*, *109*, C09S07, doi: 10.1029/2003jc001850.

[*Nakamura et al.*(2000)] Nakamura, T., T. Awaji, T. Hatayama, K. Akitomo, and T. Takizawa (2000), Tidal exchange through the Kuril Straits, *J. Phys. Oceanogr.*, *30*, 1622—1644.

[*Nakamura et al.*(2006)] Nakamura, T., T. Toyoda, Y. Ishikawa, and T. Awaji (2006), Enhanced ventilation in the Okhotsk Sea through tidal mixing at the Kuril Straits, *Deep Sea Research*, *53*, 425-448.

[*Nakamura et al.*(2010)] Nakamura, T., Y. Isoda, H. Mitsudera, S. Takagi, and M. Nagasawa (2010), Breaking of unsteady lee waves generated by diurnal tides, *Geophys. Res. Lett.*, *37*, L04,602, doi:10.1029/2009GL041456.

[*Nakamura et al.*(2012)] Nakamura, T., J. P. Matthews, T. Awaji, and H. Mitsudera (2012), Submeso-scale eddies near the Kuril Straits: Asymmetric generation of clockwise and counterclockwise eddies by barotropic tidal flow, *J. Geophys. Res.*, p. C12014, doi: 10.1029/2011JC007754.

[*Nakanowatari et al.*(2007)] Nakanowatari, T., K. Ohshima, and M. Wakatsuchi (2007), Warming and oxygen decrease of intermediate water in the northwestern North Pacific, originating from the Sea of Okhotsk, 1955—2004, *Geophys. Res. Lett.*, *34*, L04,602, doi: http://dx.doi.org/10.1029/2006GL028243.

[*Nihashi et al.*(2009)] Nihashi, S., K. I. Ohshima, T. Tamura, Y. Fukamachi, and S. Saitoh (2009), Thickness and production of sea ice in the Okhotsk Sea coastal polynyas from AMSR-E, *Journal of Geophysical Research*, *144*, C10025.

[*Nihashi et al.*(2012)] Nihashi, S., K. I. Ohshima, N. Kimura (2012), Creation of a Heat and Salt Flux Dataset Associated with Sea Ice Production and Melting in the Sea of Okhotsk. *Journal of Climate*, *25*(7), 2261–2278.

[*Nishioka et al.*(2013)] Nishioka, J., T. Nakatsuka, Y. W. Watanabe, I. Yasuda, K. Kuma, H. Ogawa, N. Ebuchi, A. Scherbinin, Y. N. Volkov, T. Shiraiwa, and M. Wakatsuchi (2013), Intensive mixing along an island chain controls oceanic biogeochemical cycles, *Global Biogeochem. Cycles*, *27*, doi:10.1002/gbc.20088.

[*Noh and Kim*(1999)] Noh, Y., and H.-J. Kim (1999), Simulations of temperature and turbulence structure of the oceanic boundary layer with the improved near-surface process, *Journal of Geophysical Research*, *104*, 15621-15634.

[*Ohshima et al.*(2002)] Ohshima, K. I., M. Wakatsuchi, Y. Fukamachi, and G. Mizuta (2002), Near-surface circulation and tidal currents of the Okhotsk Sea observed with the satellite-traced drifters, *J. Geophys. Res.*, *107(C11)*, 3195.

[*Ohshima et al.*(2004)] Ohshima, K. I., D. Simizu, M. Itoh, G. Mizuta, Y. Fukamachi, S. C. Riser, and M. Wakatsuchi (2004), Sverdrup balance and the cyclonic gyre in the Sea of Okhotsk, *J. Phys. Oceanogr.*, *34*, 513—525.

[*Ohshima et al.*(2010)] Ohshima, K. I., T. Nakanowatari, S. Riser, and M. Wakatsuchi (2010), Seasonal variation in the in- and outflow of the Okhotsk Sea with the North Pacific, *Deep Sea Research Part II: Topical Studies in Oceanography*, *57*(13—14), 1247 – 1256, doi:http://dx.doi.org/10.1016/j.dsr2.2009.12.012.

[*Okazaki et al.*(2010)] Okazaki, Y., A. Timmermann, L. Menviel, N. Harada, A. Abe-Ouchi, M. O. Chikamoto, A. Mouchet, and H. Asahi (2010), Deepwater formation in the

North Pacific during the last glacial termination, *Science*, *329*(5988), 200–204, doi: 10.1126/science.1190612.

[*Ono et al.*(2006)] Ono, J., K. I. Ohshima, G. Mizuta, Y. Fukamachi, and M. Wakatsuchi (2006), Amplification of diurnal tides over Kashevarov Bank in the Sea of Okhotsk and its impact on water mixing and sea ice, *Deep Sea Res. Part I*, *53*, 409—424.

[*Osafune and Yasuda*(2012)] Osafune, S., and I. Yasuda (2012), Numerical study on the impact of the 18.6-year period nodal tidal cycle on water masses in the subarctic North Pacific, *J. Geophys. Res.*, *117*, C05,009, doi:10.1029/2011JC007734.

[*Osafune and Yasuda*(2013)] Osafune, S., and I. Yasuda (2013), Remote impacts of the 18.6 year period modulation of localized tidal mixing in the North Pacific, *J. Geophys. Res. Oceans*, *118*, 3128—3137, doi:10.1002/jgrc.20230.

[*Sasajima et al.*(2010)] Sasajima, Y., H. Hasumi, and T. Nakamura (2010), A sensitivity study of the dense shelf water formation in the Okhotsk Sea, *J. Geophys. Res.*, *115*, C11,007, doi:10.1029/2009JC005697.

[*Schwiderski*(1980)] Schwiderski, E. W. (1980), On charting global ocean tides, *Reviews of Geophysics and space physics*, *18*(1), 243–268.

[*Shcherbina et al.*(2003)] Shcherbina, A. Y., L. D. Talley, and D. L. Rudnick (2003), Direct observations of North Pacific ventilation: brine rejection in the Okhotsk Sea, *Science*, *302*, 1952.

[*Stabeno et al.*(1994)] Stabeno, P. J., K. Reed, and J. E. Overland (1994), Lagrangian measurements in the Kamchatka Current and Oyashio, *Journal of Oceanography*, *50*, pp. 653 to 662.

[*Steele et al.*(2001)] Steele, M., R. Morley, and W. Ermold (2001), Phc: A global ocean hydrography with a high-quality Arctic Ocean, *Journal of Climate*. *14*(9), 2079.

[*Sugimoto and Hanawa*(2009)] Sugimoto, S., and K. Hanawa (2009), Decadal and interdecadal variations of the Aleutian low activity and their relation to upper oceanic variations over the North Pacific, *Journal of the Meteorological Society of Japan. Ser. II*, *87*(4), 601–614.

[*Talley and Nagata*(1995)] Talley, L., and Y. E. Nagata (1995), The Okhotsk Sea and Oyashio region (report of working group 1), *PICES Sci. Rep.*

[*Talley*(1991)] Talley, L. D. (1991), An Okhotsk Sea water anomaly: implications for ventilation in the North Pacific, *Deep Sea Research*, *38*, S171.

[*Talley*(2003)] Talley, L. D. (2003), Shallow, intermediate, and deep overturning components of the global heat budget, *J. Phys. Oceanogr.*, *33*, 530—560,

[*Tanaka et al.*(2010)] Tanaka, Y., T. Hibiya, Y. Niwa, and N. Iwamae (2010), Numerical study of K1 internal tides in the Kuril straits, *Journal of Geophysical Research*.

[*Tsujino et al.*(2000)] Tsujino, H., H. Hasumi, and N. Suginohara (2000), Deep Pacific circulation controlled by vertical diffusivity at the lower thermocline depths, *J. Phys. Oceanogr.*, *30*, 2853—2865.

[*Tsujino et al.*(2008)] Tsujino, H., H. Nakano, and T. Motoi (2008), Mechanism of currents through the straits of the Japan Sea: Mean state and seasonal variation, *Journal of Oceanography*, *64*, 141–161, doi:10.1007/s10872-008-0011-7.

[*Uchimoto et al.*(2011)] Uchimoto, K., T. Nakamura, J. Nishioka, H. Mitsudera, M. Yamamoto-Kawai, K. Misumi, and D. Tsumune (2011), Simulations of chlorofluorocarbons in and around the Sea of Okhotsk: Effects of tidal mixing and brine rejection on the ventilation, *J. Geophys. Res.*, *116*, C02,034, doi:10.1029/2010JC006487.

[*Uehara et al.*(2012)] Uehara, H., A. A. Kruts, Y. N. Volkov, T. Nakamura, T. Ono, and H. Mitsudera (2012), A new climatology of the Okhotsk Sea derived from the FERHRI database, *Journal of Oceanography*, *68*(6), 869–886, doi:10.1007/s10872-012-0147-3.

[*Uehara et al.*(2014)] Uehara, H., A. A. Kruts, H. Mitsudera, T. Nakamura, Y. N. Volkov, and M. Wakatsuchi (2014), Remotely propagating salinity anomaly varies the source of the North Pacific ventilation, *Progress in Oceanography*, accepted.

[*Watanabe et al.*(2013)] Watanabe, Y. W., J. Nishioka, and T. Nakatsuka (2013), Decadal time evolution of oceanic uptake of anthropogenic carbon in the Okhotsk Sea, *Geophys. Res. Lett.*, *40*, 322—326, doi:10.1002/grl.50113.

[*Woodgate et al.*(2005)] Woodgate, R. A., K. Aagaard, and T. J. Weingartner (2005), Monthly temperature, salinity, and transport variability of the Bering Strait through flow, *Geophysical Research Letters*, *32*, L04,601, doi:10.1029/2004GL021880.

[*Yasuda et al.*(1996)] Yasuda, I., K. Okuda, and Y. Shimizu (1996), Distribution and modification of North Pacific Intermediate Water in the Kuroshio-Oyashio interfrontal zone, *J. Phys. Oceanogr.*, *26*, 448–465.